BBA - Proteins and Proteomics 1866 (2018) 1102–1114

Contents lists available at ScienceDirect

BBA - Proteins and Proteomics

journal homepage: www.elsevier.com/locate/bbapap

# Macromolecular crowding-induced molten globule states of the alkali pH-denatured proteins

Rajesh Kumar[a,b,*], Rajesh Kumar[b], Deepak Sharma[c], Mansi Garg[a], Vinay Kumar[d], Mukesh Chand Agarwal[b]

[a] Centre for Chemical Sciences, School of Bassic and Applied Sciences, Central University of Punjab, Bathinda, 151001, India
[b] School of Chemistry and Biochemistry, Thapar University, Patiala 147004, India
[c] Council of Scientific and Industrial Research, Institute of Microbial Technology, Sector 39A, Chandigarh, India
[d] Centre for Plant Sciences, School of Bassic and Applied Sciences, Central University of Punjab, Bathinda, 151001, India

ARTICLE INFO

*Keywords:*
Molten-globule state
Crowding agents
Thermal stability
Cold denaturation
Enthalpy-entropy plot

ABSTRACT

Structural and molecular properties extracted from circular dichroism (CD), tryptophan fluorescence and 1-anilino-8-napthalene sulfonate (ANS) binding experiments suggest that the high concentration of synthetic crowding agents (dextran 40, dextran 70 and ficoll 70) stabilizes and refolds the base-denatured ferricytochrome *c* (Ferricyt *c*) and lysozyme (Lyz) at pH 12.9 ( ± 0.1) to molten globule (MG) states ($C_B$-states). These results further revealed that the $C_B$-states resemble the generic properties of MG-states. Thermodynamic analysis of thermal denaturation curves of base-denatured Ferricyt *c* and Lyz at pH 12.9 ( ± 0.1) under variable concentrations of crowding agents (dextran 40, dextran 70 and ficoll 70) revealed that the crowder presence increases the thermal stability of base-denatured proteins and also prevents the cold denaturation of Ferricyt *c*. The results further showed that the nature, size and shape of crowder influence the crowding-mediated increase in secondary structure stabilization and thermal stability of base-denatured Ferricyt *c* and Lyz. Analysis of kinetic and thermodynamic parameters measured for CO association reaction of alkaline ferrocytochrome *c* (Ferrocyt *c*) at pH 12.9 ( ± 0.1) under variable concentrations of crowding agents (dextran 40, dextran 70 and ficoll 70) revealed that the crowder presence reduces the level of structural fluctuation of M80-containing Ω-loop that control CO association to alkaline Ferrocyt *c*.

## 1. Introduction

The compaction of linear chain of amino acid residues into biologically active three-dimensional structure is a fundamental route in protein folding. In addition, one or more distinct, populated intermediates have been reported to be involved during protein folding process [1]. These intermediates have been termed as molten globule (MG)-state with key features similar to native-like molecular compaction and secondary structure but with disordered or fluctuating tertiary structure [2–8]. The MG-state was originally proposed by Ohgushi and Wada in 1983 [4]. The MG-state typically occurs mainly at the later stages but is also detected at the early stages of folding of several proteins [9–11]. It is already established that MG state like others non-native states of proteins, play a role in insertion and translocation processes of protein through organelles membranes [12–15]. The intrinsically disordered native-like proteins similar to MG-state have been found to be involved in cell signaling and work as regulator by interacting with DNA and other proteins [16–20]. Baker et al. (2005) demonstrated that a pH-dependent MG transition is necessary for the activity of the steroidogenic acute regulatory protein (StAR) that stimulates steroid synthesis [21]. Chen et al. (2011) reported that auto-inhibited homodimeric chaperones of type III secretion (TTS) adopt a molten-globule-like state that expose the substrate binding site for binding to their cognate protein substrates [22]. The conformational properties and binding mechanisms of promiscuous molten globule of murine NCBD has also been studied [23].

MG states are milieu of conformations with varying ranges of disorder, and thus it is difficult to study them under normal folding conditions at neutral pH due to their transient lifetime. However, at the extremes of pH, the MG-states are stabilized by salts [24–29]. The presence of sugars, polyols, and guanidine hydrochloride (GdnHCl) also stabilize and refold the acid-denatured state of proteins to MG states [30–33]. Recent reports showed that the MG states can also form at neutral pH without the need of denaturing conditions [34–36] and also

* Corresponding author at: Centre for Chemical Sciences, School of Bassic and Applied Sciences, Central University of Punjab, Bathinda, 151001, India.
*E-mail address:* rajesh.kumar@cup.edu.in (R. Kumar).

https://doi.org/10.1016/j.bbapap.2018.08.012
Received 23 March 2018; Received in revised form 7 July 2018; Accepted 30 August 2018
Available online 04 September 2018

in the presence of denaturant [37]. A number of studies have also shown that the high concentration of crowding agent increases the stability and structural contents of folded and partially folded proteins [38–45] as well as transforms the acid-denatured proteins to MG-states [46,47]. The crowding agent mediated excluded volume effects are predicted to favor the adoption of compact conformation as opposed to expanded macromolecular conformations, due to decrease in total excluded volume [44,45]. The crowding-induced reaction is paramount because it plays crucial role in aggregations and subsequently linked with numerous neurodegenerative disorders [47–54]. Hatter et al. (2002) documented that macromolecular crowding accelerates amyloid formation by human apolipoprotein C-II [47]. In general, crowding agents usually favor refolding of protein [55,56]. According to excluded volume theory, a non-specific force exhibits between the crowding agents and macromolecules that eventually reduces the total excluded volume and promotes the compact conformation against the expanded macromolecular conformations [57–63].

Although, the crowding-induced MG-state of acid-denatured Ferricyt *c* has been studied previously [46], the crowding-induced MG-state of base-denatured Ferricyt *c* is not explored so far. Furthermore, the crowding-induced MG-states acid- and base-denatured Lyz in the absence of denaturant have also not been investigated in detail. This is presumably because at extreme acidic pH conditions, Lyz retains its tertiary interactions. The current results show that at extreme alkaline pH conditions (pH 12.8 ( ± 0.1)), both Ferricyt *c* and Lyz lost their tertiary interactions, therefore one can characterize the crowder-induced MG-states of these proteins under basic pH conditions. Alkaline denturation of Ferricyt *c* proceeds *via* alkaline transition at pH > 9. The alkaline (pH > 9) forms of Ferricyt *c* have been identified since last 75 years [64], but remarkably their role on Ferricyt *c* function remains unclear. In the alkaline form (pH > 9), two isoforms of alkaline Ferricyt *c* exist, one of which replaces the buried $Fe^{3+}$-M80- bond by $Fe^{3+}$-Lys79 bond [64]. Earlier $^1$H NMR studies showed that $Fe^{3+}$-Lys79 bond remains in Ferricyt *c* even at extreme basic pH conditions [64]. A similarly reconfigured state may play a role in some physiologically important interactions of Ferricyt *c* at neutral pH (cytochrome oxidase [65,66], cardiolipin [67,68], lipid membranes [69,70]), therefore we have studied the crowder-induced MG-state of similarly reconfigured base-denatured Ferricyt *c*. This is the first report that revealed potential role of crowding agents (dextran 40, dextran 70 and ficoll 70) in transformation of the base-denatured Ferricyt c and Lyz into their respective MG-states *i.e.* $C_B$-states at pH 12.8 ( ± 0.1). The fully populated $C_B$-states meet the generic properties of MG-state, *i.e.*, molecular compact state with native-like secondary structure but lacks tertiary structure. Thermodynamic analysis of thermal denaturation curves of base-denatured Ferricyt c and Lyz at pH 12.9 ( ± 0.1) carried out at different concentrations of crowding agents (dextran 40, dextran 70 and ficoll 70) revealed that (i) presence of the crowding agent in the reaction medium increases the thermal stability of base-denatured proteins, and (ii) the extent of crowding-mediated increased thermal stability of base-denatured proteins depends on the concentration, nature and shape of crowding agents.

Analysis of kinetic and thermodynamic parameters measured for CO-association reactions of alkaline Ferrocyt *c* at pH 12.9 ( ± 0.1) in the presence of different concentrations of crowding agents (dextran 40, dextran 70 and ficoll 70) revealed that (i) the crowder presence decreases the level of structural fluctuation that control CO association to base-denatured of Ferrocyt *c*, and (ii) the crowding-mediated decrease in the level of structural fluctuation of base-denatured Ferrocyt *c* depends on the nature and shape of crowding agents or on size of crowding agents of similar shape.

## 2. Materials and methods

Horse heart cytochrome *c* (Cyt *c*; type VI), crowding agents (dextran 40, dextran 70 and ficoll 70), salts of buffer (sodium phosphate, Tris-base and 3-[Cyclohexylamino]-1-propanesulfonic acid (CAPS), sodium dithionite and 1-anilino-8-napthalene sulfonate (ANS)) were purchased from Sigma. Hen egg white lysozyme (Lyz) was purchased from Calbiochem. Chemical denaturants (guanidine hydrochloride (GdnHCl) and urea) were purchased from USB (USA). All other chemicals used in this study were of analytical grade. The pH of samples was adjusted by using the concentrated HCl and NaOH solutions. The concentrations of GdnHCl and urea stock solutions were determined by refractive index measurements by using an Abbe's Refractometer (Thermo scientific). The kinetics and thermodynamic data were analyzed by using Sigma Plot (v. 9) and Origin software (MicroCal Inc.).

### 2.1. Measurement of pH-titrations of Ferricyt c and Lyz

For pH unfolding studies of Ferricyt *c* and Lyz, the protein samples were prepared in buffer containing 10 mM of Tris, 10 mM of disodium hydrogen phosphate and 2 mM CAPS. The pH of protein samples was adjusted from 7.0–13.2 range. The titration was carried out without disturbing the uniformity of the protein concentration and incubated for ~40 min. The fluorescence (excitation: 280 nm) emission (310–400 nm) and far-UV CD spectra (250–200 nm) were recorded on Perkin Elmer LS-55 or PTI QM 40 (Photon Technology) fluorescence spectrophotometer and JASCO-810 spectropolarimeter, respectively at 25 °C. The fluorescence and far-UV CD data were normalized using Eq. (1)

$$Y_{obs} = [(Y - Y_N)/(Y_U - Y_N)] \quad (1)$$

where, $Y_{obs}$ is the observed value of the CD or fluorescence signal, $Y_N$ and $Y_U$ are the CD or fluorescence signal intensities for the native (pH 7.0) and pH-denatured (pH 12.9) states, respectively. The pH titration curves were analyzed by using the following transformed Henderson-Hasselbalch Eq. (2) [24],

$$Y_{obs} = \left[\frac{C_u + C_f\,[10^{n(pH-C_m)}]}{1 + 10^{(pH-C_m)}}\right] \quad (2)$$

where, $C_u$ and $C_f$ show the signals for the unfolded and the folded states, respectively, $n$ defines the number of $OH^-$ ions titrated, and $C_m$ denotes the pH-midpoint for the transition.

### 2.2. Measurement of the far-UV CD, near-UV CD and fluorescence emission spectra of Ferricyt c and Lyz

The far-UV (200–250 nm, 1.0 mm cell) and near-UV (250–300 nm, 5.0 mm cell) CD spectra of Ferricyt *c* and Lyz were collected at pH 7.0 (50 mM sodium phosphate buffer) and pH 12.9 ( ± 0.1) (2 mM CAPS buffer) in the absence and presence of different concentrations of crowding agents (dextran 40, dextran 70 and ficoll 70) on JASCO 815 spectropolarimeter at 25 °C. The optimized concentration of proteins for the far-UV and near-UV CD experiments was ~12 μM and ~60 μM, respectively. All CD spectrum of Ferricyt *c* and Lyz were corrected by subtracting the CD spectra of the corresponding blank solutions of a particular concentrations of crowding agents (dextran 40, dextran 70 and ficoll 70) at pH 12.9 ( ± 0.1), 25 °C. Similarly, the Trp fluorescence (ex: 280 nm) emission spectra (310–420 nm, 10 mm path length cuvette; 5 μM protein) of Ferricyt *c* and Lyz were collected at pH 7 (50 mM sodium phosphate buffer) and pH 12.9 ( ± 0.1) (2 mM CAPS buffer) with control and presence of different concentrations of crowding agents on Perkin Elmer LS-55 or PTI QM 40 (Photon Technology) fluorescence spectrophotometer at 25 °C. In addition, ANS emission spectra (ex: 380 nm, em: 400–600 nm) of Ferricyt *c* and Lyz were also collected using Perkin Elmer LS-55 or PTI QM 40 (Photon Technology) fluorescence spectrophotometer. For ANS fluorescence measurements, ratio of ANS (0.5 mM) and protein (5 μM) were maintained at 100:1.

### 2.3. Measurement of $^1$H NMR spectra for different states of Ferricyt c and Lyz

For preparation of native states, $D_2O$ solution containing 1.0 mM protein (Ferricyt c or Lyz) was adjusted to pH 7.0 (0.05 M phosphate) using concentrated DCl or NaOD. For preparation of base-denatured states, $D_2O$ solution containing 1.0 mM protein (Ferricyt *c* or Lyz) and 1.0 mM CAPS, was adjusted to pH 12.9 ( ± 0.1) using concentrated NaOD. For preparation of salt or crowding induced MG-states, 2.0 M NaCl or 300 mg ml$^{-1}$ crowding agent was added in $D_2O$ solution containing 1.0 mM protein (Ferricyt c or Lyz) and 1.0 mM CAPS, and the pH was adjusted to 12.9 ( ± 0.1) using concentrated NaOD.

### 2.4. Measurement of thermal denaturation of Ferricyt c and Lyz under various concentrations of crowding agents

To determine the effect of crowding agents on thermal denaturation of base-denatured proteins, the far-UV CD (222 nm) monitored thermal denaturation curves of Ferricyt *c* and Lyz were collected at pH 12.9 ( ± 0.1) under varying concentrations of crowding agents (dextran 40. dextran 70, ficoll 70) on JASCO-815 spectropolarimeter. The protein concentration for melting experiments was ~10–15 μM. The Peltier-controlled heating rate was maintained at 1.0 °C/min. By assuming a two-state denaturation process, the thermal denaturation data were analyzed by Gibbs Helmholtz Eq. (3) [24],

$$y(T) = \frac{(y_F + m_F T) + (y_D + m_D T)\exp\left(\frac{\Delta H_m\left(\frac{T}{T_m}-1\right) - \Delta C_p\left(T_m - T + T\ln\left(\frac{T}{T_m}\right)\right)}{RT}\right)}{1 + \exp\left(\frac{\Delta H_m\left(\frac{T}{T_m}-1\right) - \Delta C_p\left(T_m - T + T\ln\left(\frac{T}{T_m}\right)\right)}{RT}\right)} \quad (3)$$

where $y$(T) is the observed variable parameter ($CD_{222\ nm}$), $y_F$ and $y_D$, and $m_F$ and $m_D$, represent intercepts and slopes of the pretransition and post-transition baselines respectively; $T$ represents absolute temperature; $\Delta C_p$ denotes heat capacity change; $R$ represents gas constant, and $\Delta H_m$ represents the van't Hoff enthalpy at thermal denaturation midpoint ($T_m$).

### 2.5. Measurement of kinetics of CO association with Ferrocyt c under various concentrations of crowding agents

CO-association kinetics with Ferrocyt *c* (Ferrocyt *c* + CO → Ferrocyt *c*-CO) was carried out using previously described methods with minor modifications [27]. A fixed amount of Ferricyt *c* was dissolved in 50 mM phosphate buffer at pH 7.0 and reduced with sodium dithionite under dry $N_2$ atmosphere. About 30 μl of the reduced protein solution was added to 2 ml of deaerated CO saturated (~1.0 mM) desired pH buffer containing sodium dithionite and varying concentrations of crowding agents at pH 7.0 and pH 12.9 ( ± 0.1). Inset of panel (a) presents the steady-state visible absorption spectra of Ferrocyt *c* and Ferrocyt *c*-CO at 25 °C, pH 12.9 ( ± 0.1) (Fig. 8a). The maximum of α band (heme π → π*) at 550 nm is corresponding to $Fe^{2+}$-M80 axial coordination of the Ferrocyt *c*. Furthermore, the CO interaction with Ferrocyt c replaces the native $Fe^{2+}$–M80 bond by non-native $Fe^{2+}$–CO bond [27,71,72]. Thus, the CO-association kinetics for Ferrocyt *c* was recorded by monitoring the decrease in absorbance at 550 nm, at 25 °C on Shimadzu (UV- 2450) spectrophotometer. The final concentrations of protein and sodium dithionite in CO association kinetic experiments were ~12 μM and ~3.0 mM, respectively.

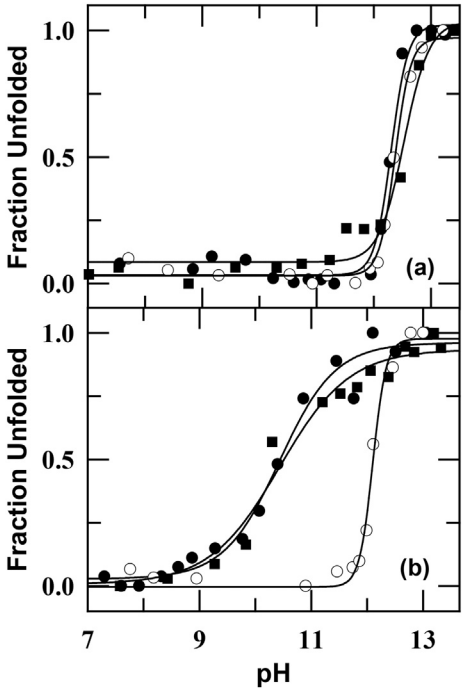


**Fig. 1.** Panels (a) and (b) represent the normalized fluorescence (●), far-UV CD (222 nm) (○) and near-UV CD (282 nm) (■) monitored alkaline pH-unfolding curves for Ferricyt *c* and Lyz, respectively at 25 °C. Solid lines in panel (a) and (b) are fit according to transformed Handerson-Hasalbalch equation (eq. (2)) [24] at 25 °C.

## 3. Results and discussion

### 3.1. Alkaline pH condition induces denaturation of Ferricyt c and Lyz

Earlier pH-dependent fluorescence studies of Ferricyt *c* and Lyz revealed that these proteins unfold at pH ≥ 12.9 [71–78]. The normalized fluorescence-monitored pH-unfolding curves of Ferricyt *c* and Lyz are shown in Fig. 1a and b, respectively at 25 °C. In case of Lyz, the emission wavelength shift is more informative than emission intensity so the fraction unfolded for Lyz was estimated from emission wavelength shift rather than emission intensity. Fig. 1a and b also show the far-UV CD (222 nm) and near-UV CD (282 nm) monitored pH-unfolding curves of Ferricyt *c* and Lyz, respectively at 25 °C. The far-UV CD, near-UV CD and fluorescence-monitored pH-unfolding curves of Ferricyt *c* are not much distinct (Fig. 1a). However, the far-UV CD-monitored pH-unfolding curve of Lyz shifts to higher pH than the fluorescence and near-UV CD monitored unfolding curves (Fig. 1b). The non-coincidence pH mediated transitions of Lyz monitored by far-UV CD and fluorescence/near-UV CD is due to existence of equilibrium intermediate between the native and denatured state transition [78]. An earlier study by Owais and co-workers also showed that the Lyz exists as a monomer at pH range from 7 to 12.6 [78]. An earlier report by Nakamura et al. showed the presence of an equilibrium intermediate in the native to denatured state transition of Ferricyt *c* at acidic pH ~4.1 [25]. The pH titration curves of Ferricyt *c* and Lyz were analyzed by using the modified Handerson-Hasalbalch equation (Eq. (1)) [24] which helps to determine the pH-midpoint, ($c_m$) and the number of $OH^-$ titrated ($n$) (Table 1). The different values of $C_m$ by far-UV CD and fluorescence or near-UV CD titration of Lyz (Fig. 1b and Table 1) confirms the existence of an equilibrium intermediate in the native to denatured state transition. However, the difference in midpoints in the curves representing far-UV CD and fluorescence or near-UV CD signals is only ≤0.2 pH unit for Ferricyt *c* (Fig. 1a and Table 1), suggesting that there is no accumulation of intermediates to a detectable level in the alkali unfolding of

**Table 1**
Fluorescence (exitation.280; emission 365) and far-UV CD (222 nm) monitored pH-induced denaturation midpoint, ($c_m$) for Ferricyt *c* and and Lyz.

| | Trp fluorescence | | far-UV CD (222 nm) | | near-UV CD (282 nm) | |
|---|---|---|---|---|---|---|
| | pH-midpoint (*C*m) | Number of $OH^-$ titrated (*n*) | pH-midpoint (*C*m) | Number of $OH^-$ titrated (*n*) | pH-midpoint (*C*m) | Number of $OH^-$ titrated (*n*) |
| Ferricyt *c* | 12.3 | 3.0 | 12.4 | 3.2 | 12.5 | 2.0 |
| Lyz | 10.4 | 0.9 | 12.1 | 3.6 | 10.4 | 0.8 |

Ferricyt *c*. The number of $OH^-$ titrated by fluorescence and far-UV CD-monitored pH titration of Ferricyt *c* are almost same and roughly equal to three $OH^-$ as shown in Table (1). In contrast, the number of $OH^-$ titrated by far-UV CD and fluorescence or near-UV CD- monitored pH titrations of Lyz are different and roughly three and one $OH^-$, respectively (Table 1).

### 3.2. Role of macromolecular crowding fluorescence emission spectra of base-denatured Ferricyt c and Lyz

The single tryptophan, W59 of Ferricyt *c* is typically buried in the hydrophobic core and almost no fluorescence signal is detected (fluorescence-silent) for native state [75,76]. However, during denaturation process, significant increase in fluorescence intensity of Ferricyt *c* has been observed [75,76]. Some previous studies revealed that the alkaline pH-denaturation of Lyz (contain 6 aromatic amino acids) caused a rapid decrease in fluorescence intensity with red shift presumably because of exposure of tryptophan residues to the polar solvent and ionization of certain tyrosine groups [77,78]. The effects of crowding agents (dextran 40, dextran 70 and ficoll 70) on the tryptophan fluorescence emission spectrum of base-denatured Ferricyt *c* and Lyz (pH 12.9 ( ± 0.1) ($U_B$-state)) are shown in Fig. 2a and Fig. 2b, respectively. For comparison purpose, the tryptophan fluorescence emission spectra of native Ferricyt *c* and Lyz (pH 7.0) are also shown in Fig. 2a and Fig. 2b, respectively. The data in Fig. 2a and Fig. 2b clearly show that the intensity and $\lambda_{max}$ of tryptophan fluorescence emission as observed for the $U_B$-states of Ferricyt *c* (Fig. 2a and Table S1) and Lyz (Fig. 2b and Table S1) is decreased and red shifted, respectively, in the presence of ~300 mg $ml^{-1}$ concentration of crowding agent (dextran 40, dextran 70 and ficoll 70). The crowding-mediated decrease in fluorescence intensity of base-denatured Ferricyt *c* (Fig. 2a) and Lyz (Fig. 2b) suggests that crowding agents might shift equilibrium between the denatured and molten globule states. The crowded-mediated red shift in $\lambda_{max}$ of base-denatured Ferricyt *c* (Fig. 2a and Table S1) and Lyz (Fig. 2b and Table S1) indicates that tryptophan gets more exposed to the polar solvent upon inclusion of crowding agents to the base-denatured proteins.

Under solution conditions, ficoll is regarded as a spherical shaped crowder while dextran as a rod-shaped [79]. The three crowding agents used here are related by Stokes radii in the order: dextran 70 (58 Å) > ficoll 70 (49.5 Å) > dextran 40 (45 Å) (http://tdbcons.com/images/pdf/FITCFicoll.pdf.). The extent of crowding-mediated decrease in tryptophan fluorescence emission intensity of base-denatured Ferricyt *c* and Lyz (Fig. 2a and Fig. 2b) typically follows the order: dextran 40 > dextran 70 > ficoll 70 (Fig. 2a and Fig. 2b), suggesting that nature and shape of crowding agents or size of crowding agents of similar shape modulate the local environment of the aromatic side chains of base-denatured proteins, especially their solvation. It was earlier reported that presence of salt also decreases the tryptophan fluorescence emission intensity of the base-denatured proteins [24,27–29]. Data in Fig. 2a and Fig. 2b indicate that presence of salt in reaction medium decreases the tryptophan fluorescence emission intensity of base-denatured Ferricyt *c* and Lyz.

Traditionally, ANS, an extrinsic fluorescent probe that binds to exposed hydrophobic clusters of folding intermediates is widely used to detect the MG-states of proteins [80–85]. The ANS fluorescence

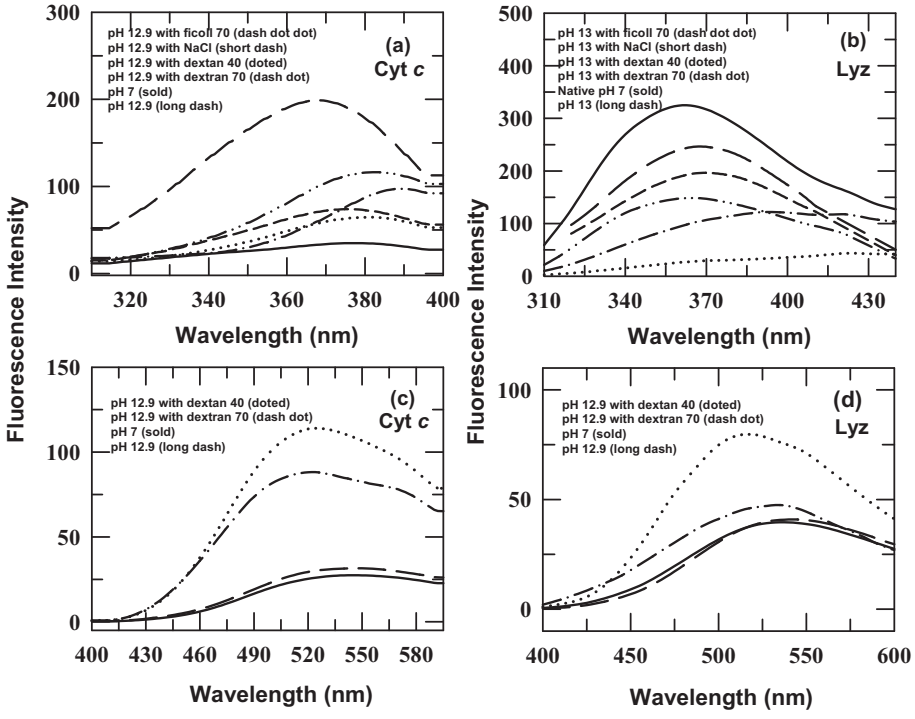


**Fig. 2.** Panels (a) and (b) represent Trp-fluorescence emission spectra of Ferricyt *c* and Lyz, respectively for different states at 25 °C: (solid line) pH 7.0, native state; (long dash line) pH 12.9 ( ± 0.1) unfolded state; (doted line) pH 12.9 ( ± 0.1) with 300 mg $ml^{-1}$ dextran 40; (dash dot line) pH 12.9 ( ± 0.1) with 300 mg $ml^{-1}$ dextran 70; (dash dot dot line) pH 12.9 ( ± 0.1) with 300 mg $ml^{-1}$ ficoll 70 (short dash line) pH 12.9 ( ± 0.1) with 2.0 M salt (2.0 M NaCl (panel (a)) and 2.0 M KCl (panel (b))). Panels (c) and (d) represent the ANS-fluorescence emission spectra of Ferricyt *c* and Lyz, respectively for different states at 25 °C: (solid line) pH 7.0, native state; (long dash line) pH 12.9 ( ± 0.1) unfolded state; (doted line) pH 12.9 ( ± 0.1) with 300 mg $ml^{-1}$ dextran 40; and (dash dot line) pH 12.9 ( ± 0.1) with 300 mg $ml^{-1}$ dextran 70.

intensity of MG-state is generally higher than the native and unfolded states of proteins [80–85]. The stronger affinity of ANS with MG-state is because of lack of rigid packing of hydrophobic clusters in MGs (Fig. 2c and Fig. 2d). The solvent accessible hydrophobic core was found to be completely absent in the denatured or unfolded proteins (Fig. 2c and Fig. 2d) [85]. Thus, the probe shows least binding affinity to unfolded states of protein.

The ANS fluorescence spectra of native Ferricyt *c* and Lyz, are shown in Fig. 2c and Fig.2d, respectively at 25 °C, pH 7.0. Fig. 2c and Fig.2d also show the ANS fluorescence spectra of base-denatured Ferricyt *c* and Lyz at pH 12.9, respectively in the absence and presence of ~400 mg ml$^{-1}$ crowding agent (dextran 40 and dextran 70). The data clearly show increased ANS fluorescence intensity of base-denatured Ferricyt *c* and Lyz in the presence of crowding agent as compared to in the absence of crowding agent was absent (Fig. 2c and Fig. 2d). This observation indicates the role of crowding agent in reaction medium for transformation of the base-denatured Ferricyt *c* and Lyz to MG-states.

Control experiments such as ANS fluorescence without protein in the absence and presence of ~ 300 mg ml$^{-1}$crowding agents (dextran 40, dextran 70 and ficoll 70) revealed that the ficoll 70 increases ANS fluorescence intensity significantly (Fig. S1), indicating that ANS may interact with ficoll 70. An unusual increase of the ANS fluorescence intensity by ficoll 70 even without protein precludes us to study the ANS fluorescence of base-denatured proteins in the presence of ficoll 70.

### 3.3. Macromolecular crowding and salt transform the base-denatured Ferricyt c and Lyz to generic molten globule states

Far-UV CD spectrum (peptide CD) in the region 200–250 nm is generally used to monitor the secondary structures of proteins [86,87]. Interestingly, the MGs are also identified by acquiring the native-like far-UV CD signals [80–88]. The far-UV CD spectra of native Ferricyt *c* and Lyz at pH 7.0 are shown in Fig. 3a and Fig. 3b, respectively. The far-UV CD spectra of native Ferricyt *c* and Lyz at pH 7.0 exhibit two negative bands (208 and 222 nm) as shown in Fig. 3a and Fig. 3b, that reflect existence of α-helical secondary structure in native proteins [89]. The far-UV CD spectrum of base-denatured Ferricyt *c* and Lyz collected in the absence and presence of 300 mg ml$^{-1}$ of crowding agents at pH 12.9 ( ± 0.1) are also shown in Fig. 3a and Fig. 3b, respectively. For comparison, these figures also present far-UV CD spectra of Ferricyt *c* and Lyz, respectively, at pH 7 in the presence of 5.0 M GdnHCl. The peptide bonds in the far-UV CD spectrum of Ferricyt *c* and Lyz were found to be disrupted significantly in the absence of denaturant at pH 12.9 ( ± 0.1) and interestingly in the presence of 5.0 M GdnHCl at pH 7 (Fig. 3a and Fig. 3b). These observations reveal that the secondary structures of Ferricyt *c* and Lyz were significantly lost in the absence of denaturant at pH 12.9 ( ± 0.1) and in the presence of GdnHCl at pH 7.0. When ~400 mg ml$^{-1}$ crowding agents (dextran 40, dextran 70 and ficoll 70) is added individually in different set of the base-denatured Ferricyt *c* and Lyz at particular pH (12.9; ± 0.1), the base-denatured proteins were found to acquire the native-like peptide bands (Fig. 3a and Fig. 3b). This finding reveals that the high concentration of crowding agent induced the native-like secondary structures in the base denatured proteins. The possible reason for native-like secondary structure stabilization of base-denatured proteins by synthetic crowders is that dextran and ficoll are inert and non-reactive to protein but occupy the large space in the reaction medium along with protein of interest. Thus, inert crowding agent decreases the volume available for protein, thus favoring the more compact state over the more expanded base-unfolded state for protein.

The near UV CD signals originate due to environments of aromatic amino acid side chain (phenylalanine, tyrosine and tryptophan) and presence of disulphide bonds in protein. Near UV CD signals between 250 and 270 nm, 270–290 nm and 280–300 nm are attributable to phenylalanine residues, tyrosine, and tryptophan [86,87]. Disulfide bonds produce broad weak signals throughout the near-UV spectrum. The presence of significant content of these near-UV signals is a reliable assay to describe that the protein is in a folded conformation with a well-defined structure. When a protein retains secondary structure but does not acquire well defined three-dimensional structure (*i.e.,* incorrectly folded or "molten-globule" structure), the signals in the near-UV region will be nearly zero. The near-UV CD signals are also sensitive to small changes in tertiary structure because of protein-protein interactions and/or changes in solvent conditions. The rigidity of the protein and nature of the environment in terms of hydrogen bonding, polar groups and polarisability can also affect the near-UV CD signals.

A dramatic loss of near-UV CD signal helps to identify the MGs of

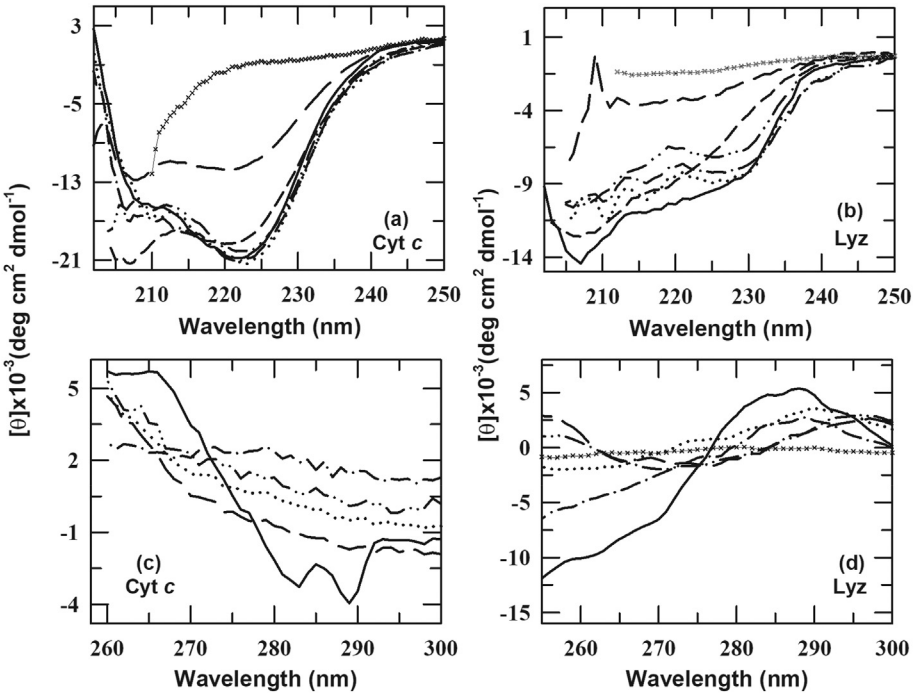


**Fig. 3.** Panels (a) and (b) represent the far-UV CD spectra of Ferricyt *c* and Lyz, respectively for different states at 25 °C: (solid line) pH 7.0, native state; (long dash line) pH 12.9 ( ± 0.1) unfolded state; (doted line) pH 12.9 ( ± 0.1) with 400 mg ml$^{-1}$ dextran 40; (dash dot line) pH 12.9 ( ± 0.1) with 400 mg ml$^{-1}$ dextran 70; (dash dot dot line) pH 12.9 ( ± 0.1) with 400 mg ml$^{-1}$ ficoll 70; (short dash line) pH 12.9 ( ± 0.1) with 2.0 M salt (2.0 M NaCl (panel (a)) and 2.0 M KCl (panel (b))); and (cross line line) pH 7, 5.0 M GdnHCl. Panels (c) and (d) represent the near-UV CD spectra of Ferricyt *c* and Lyz, respectively for different states at 25 °C: (solid line) pH 7.0, native state; (long dash line) pH 12.9 ( ± 0.1) unfolded state; (dotted line) pH 12.9 ( ± 0.1) with 400 mg ml$^{-1}$ dextran 40; (dash dot line) pH 12.9 ( ± 0.1) with 400 mg ml$^{-1}$ dextran 70; (dash dot dot line) pH 12.9 ( ± 0.1) with 400 mg ml$^{-1}$ ficoll 70; and (cross line line) pH 7 ( ± 0.1) with 5.0 M GdnHCl (only panel (d)).

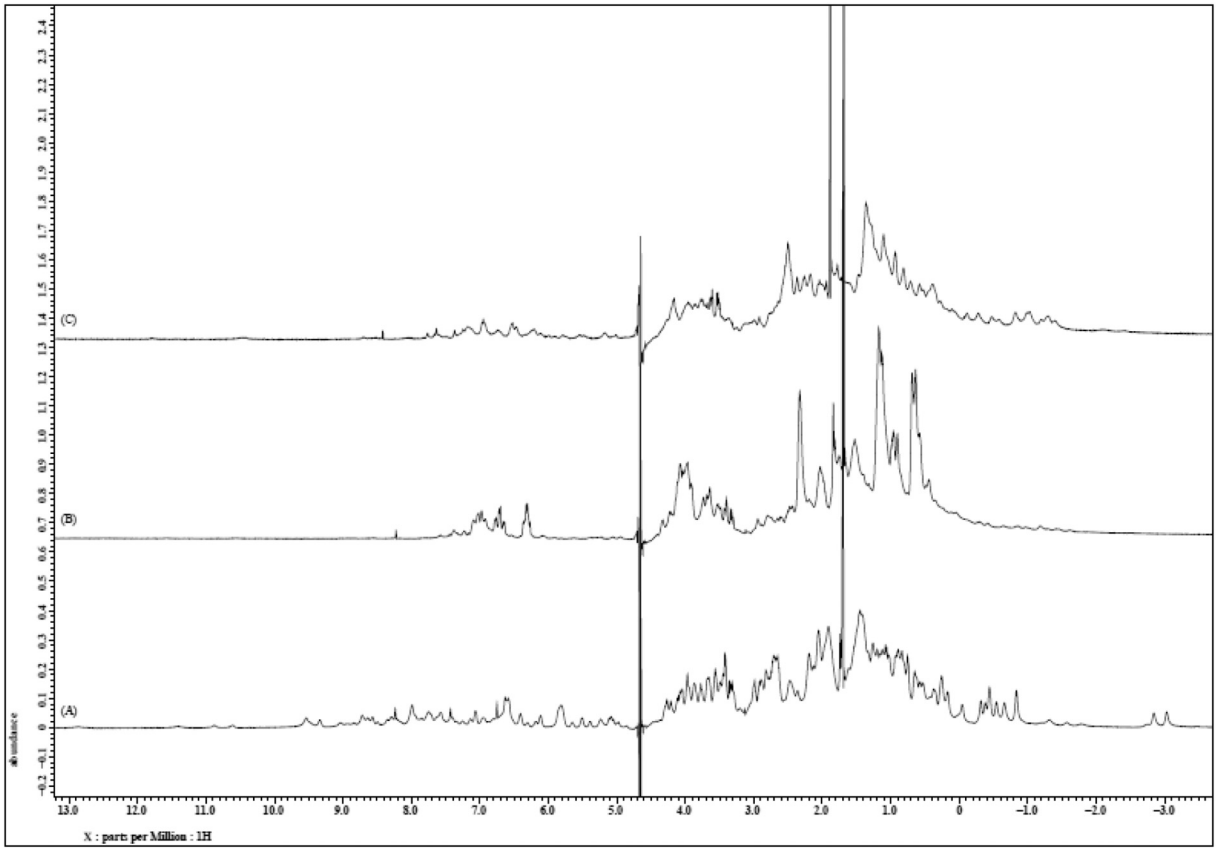


**Fig. 4.** $^{1}$H NMR spectra for the different states of ferricyt *c*. Panels (A) and (B) present the $^{1}$H NMR spectra for native state of Ferricyt *c* at pH 7.0 and base-denatured state of Ferricyt *c* at pH 12.9 ( ± 0.1), respectively at 25 °C. Panel (C) present the $^{1}$H NMR spectra of salt-induced MG-state of base-denatured Ferricyt *c* at pH 12.9 ( ± 0.1), 25 °C. For clarity, only selected regions of aromatic, aliphatic and heme substituent resonances are shown.

particular protein [80–88]. The relevant aromatic CD spectra of different states of Ferricyt *c* and Lyz are shown in Fig. 3c and Fig. 3d, respectively. At pH 12.9 ( ± 0.1), the signals due to aromatic amino acids subsequently responsible for tertiary structure has been found to be significantly lost (Fig. 3c and Fig. 3d). After adding ~400 mg ml$^{-1}$ crowding agent (dextran 70 and ficoll 70) in the base-denatured Ferricyt *c* and Lyz separately at same pH condition, the base-denatured proteins were absent of aromatic band (Fig. 3c and Fig. 3d). In conclusion, the inclusion of higher concentration of crowding agent was found unable to induce the tertiary structures in already base denatured Ferricyt *c* and Lyz.

A regiospecific spectroscopic technique, such as $^{1}$H NMR spectroscopy can be used to characterize the native, base-denatured and MG-states of Ferricyt *c* and Lyz [90]. In general, the native state of protein is characterized by narrow and well dispersed resonances while the unfolded or base-denatured state is differentiated by significant loss in both lineshape and chemical shift dispersion. By definition, the MG-state exhibits increased internal mobility and side-chain environmental averaging [2,4]. At pH 7.0, Ferricyt *c* and Lyz are in native states and the $^{1}$H NMR lines for these are narrow and well dispersed (Fig. 4A and Fig. 5A). Upon increase in pH from pH 7.0 to 12.9 ( ± 0.1), the proteins denature as indicated by the loss of both chemical shift dispersion and lines shapes (Fig. 4B and Fig. 5B). When 2.0 M salt is added in the base-denatured Ferricyt *c* and Lyz, the spectrum partly regains dispersion as well as sharpness of resonances, shown for the aliphatic and resonances (Fig. 4C and Fig. 5C). Relative to native state resonances, the salt-induced MG-states resonances of base-denatured Ferricyt *c* and Lyz are still not noticeably broad, indicating that salt-induced MG-states of these proteins are not markedly mobile and retains some traces of tertiary structures. To test whether $^{1}$H NMR spectrums of base-denatured Ferricyt *c* and Lyz also partly regain dispersion as well as sharpness of resonances in the presence of high concentration of crowding agent, we have collected the $^{1}$H NMR spectrums of base-denatured Ferricyt *c* and Lyz in the presence of 300 mg ml$^{-1}$ crowding agent. Unfortunately, we are unable to characterize the crowding-induced MG-states of base-denatured Ferricyt *c* and Lyz by NMR spectroscopy because the crowder presence suppressed the base-denatured proteins NMR peaks (Fig. S2).

### 3.4. Macromolecular crowding-induced refolding in the base-denatured Ferricyt c and Lyz

Fig. 6a and Fig. 6b show the change in far-UV CD ellipticity at 222 nm with [Crowding agents] for the base-denatured Ferricyt *c* and Lyz, respectively at pH 12.9 ( ± 0.1), 25 °C. The data in Fig. 6a and Fig. 6b clearly suggest that the crowder environment induces the transformation of the base-denatured Ferricyt *c* and Lyz ($U_B$-state) into $C_B$-states at 25 °C. It is surprising to observe sharp cooperative transitions between base-unfolded and crowder-induced molten globule states of Ferricyt *c* and Lyz (Fig. 6a and Fig. 6b). This is in agreement with some of the previous studies where high cooperativity in the transitions between acid/base-unfolded and salt-induced MG-states of Ferricyt *c* has also been observed [88,91,92]. MGs in certain cases also have been found to show cooperative thermal unfolding transitions for Ferricyt *c*, apoMb, staphylococcal nuclease, equine Lyz, and canine milk Lyz [3,24]. The Gibbs free energy change, $\Delta G$, for the two-state transition, $U_B \rightarrow C_B$ can be calculated by the eq. (4) given as:

$$\Delta G = -RTInK = -RTIn\left[(Y_{obc} - Y_{Ug})/(Y_{Cg} - Y_{obs})\right] \quad (4)$$

where, $Y_{obs}$ shows the observed value of the CD signal, $Y_{UB}$ and $Y_{CB}$ represents the corresponding values for the $U_B$ and $C_B$-states, respectively. The $\Delta G$ *vs.* [Crowding agents] plots for refolding of Ferricyt *c* and

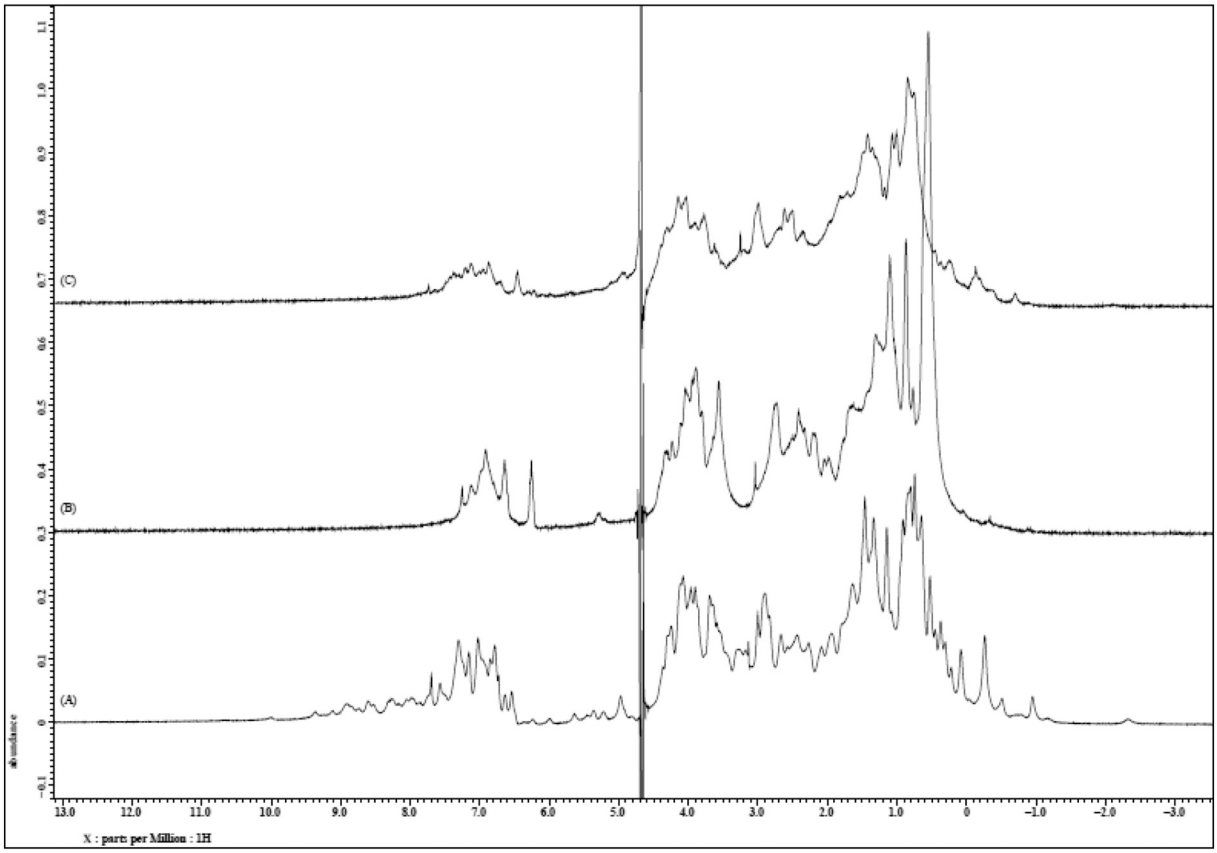


**Fig. 5.** $^{1}$H NMR spectra for the different states of Lyz. Panels (A) and (B) present the $^{1}$H NMR spectra for native state of Lyz at pH 7.0 and base-denatured state of Lyz at pH 12.9 ( ± 0.1), respectively at 25 °C. Panel (C) present the $^{1}$H NMR spectra of salt-induced MG-state of base-denatured Lyz at pH 12.9 ( ± 0.1), 25 °C. For clarity, only selected regions of aromatic, aliphatic and heme substituent resonances are shown.

Lyz are shown in Fig. 6c and Fig. 6d, respectively. On the assumption of a linear dependence of $\Delta G$ on [Cosolute] concentration [93], the least-squares fit of the data to eq. (5), provides the values of $\Delta G^{o}$ and $m$ (slop reflecting the cooperatively of the transition) (Table 2)

$$\Delta G = \Delta G^{0} - m[Crowding\ agents] \quad (5)$$

For selected protein(s), the $\Delta G^{o}$ values for dextran 40, dextran 70 and ficoll 70 are within error identical (Table 2). The estimated $m$-values (which reflect the concentration dependent effects of the crowders) are also not greatly different for dextran 40, dextran 70 and ficoll 70

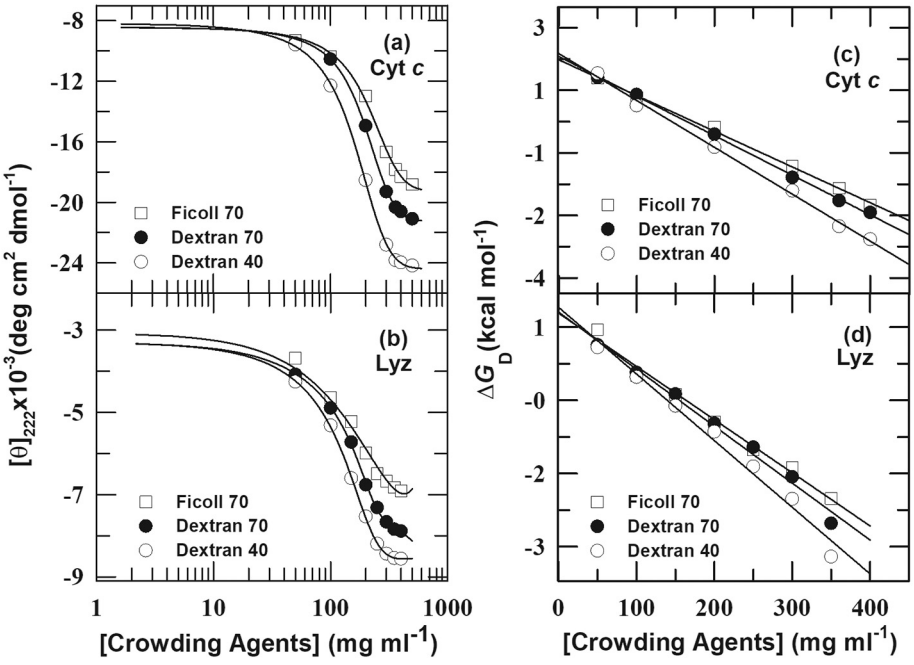


**Fig. 6.** Panels (a) and (b) represent the change of mean residue ellipticity (222 nm) of Ferricyt *c* and Lyz, respectively with [crowding agents] (dextran 40 (o) dextran 70 (●) and ficoll 70 (□)) at pH 12.9 ( ± 0.1). The continuous lines are just guide to the eye. Panel (c) and (d) represent the plots of $\Delta G$ with [crowding agents] (dextran 40 (o) dextran 70 (●) and ficoll 70 (□)) for refolding of base-denatured Ferricyt *c* and Lyz, respectively at pH 12.9 ( ± 0.1). The least-squares fit of the data to Eq. (5) (panels (c) and (d)), provides the values of $\Delta G^{o}$ and $m$ (Table 2).

**Table 2**
Thermodynamic parameters, free energy ($\Delta G^o$) and $m$ (slop) for the refolding (CD 222 nm) of base-denatured proteins (Ferricyt *c* and Lyz) in the presence of crowding agents at pH 12.9 ( ± 0.1), 25 °C.

| Crowding agents | $\Delta G^o$ (kcal mol$^{-1}$) | $m$ (kcal mol$^{-1}$ M$^{-1}$) |
|---|---|---|
| Ferricyt *c* | | |
| dextran 40 | 1.88 (0.1) | 0.01 |
| dextran 70 | 1.81 (0.1) | 0.0094 |
| ficoll 70 | 1.73 (0.1) | 0.0086 |
| Lyz | | |
| dextran 40 | 1.70 (0.1) | 0.0137 |
| dextran 70 | 1.61 (0.1) | 0.012 |
| ficoll 70 | 1.59 (0.1) | 0.011 |

(Table 2). These findings suggest that the effectiveness of the crowding towards refolding of base-denatured proteins to MG-states does not vary significantly with different crowders. Although, the observed ellipticity (222 nm) in the far-UV CD spectra of base-denatured proteins for dextran 40, dextran 70 and ficoll 70 vary quite significantly (Fig. 6a and Fig. 6b), these difference may just reflect differences in the baselines at the highest concentrations (Fig. 6a and Fig. 6b), and may have little to do with differences in the conformational ensembles of the proteins.

### 3.5. Role of macromolecular crowding on heat and cold denaturations of base-denatured proteins

To investigate the role of hydrophobic interactions and macromolecular crowding on thermal denaturations of base-denatured proteins, the far-UV CD monitored (222 nm) thermal denaturation curves of Ferricyt *c* and Lyz were collected at pH 12.9 ( ± 0.1) in the absence and presence of ~ 300 mg ml$^{-1}$ of crowders (Fig. 7a and Fig. 7b). The low temperature ellipticity values varied with concentration of crowding agent while no similar change was observed at high-temperature (Fig. 7a and Fig. 7b). The thermal denaturation data for base-denatured Ferricyt *c* and Lyz were normalized using Eq. (6)

$$Fraction\ Unfolded = [(\theta - \theta_N)/(\theta_U - \theta_N)] \quad (6)$$

where, $\theta$ is the observed value of ellipticity (222 nm) at given temperature, $\theta_N$ and $\theta_U$ are the most negative and least negative or positive value of ellipticity (222 nm) in thermal transition curve. The normalized thermal unfolding curves for Ferricyt *c* and Lyz are shown in Fig. 7a and Fig. 7b, respectively. An earlier report revealed that the thermal denaturation of base-denatured Ferricyt *c* at pH 12.9 in the presence of salt exhibits reversibility [24]. To ascertain that the thermal denaturations of base-denatured Ferricyt *c* and Lyz at pH 12.9 ( ± 0.1) also exhibit reversibility in presence of crowding agent, the base-denatured Ferricyt *c* and Lyz at pH 12.9 ( ± 0.1) in presence of 100 mg ml$^{-1}$ dextran 70 were heated gradually from 273 K to 323 K for Ferricyt *c* and 294 K to 345 K for Lyz, and cooled down gradually to 273 K from 323 K for Ferricyt *c* and to 294 K from 345 K for Lyz. The forward-scan and reverse-scan in Fig. S3a are nearly superimposable, suggesting that thermal transition for base-denatured Ferricyt *c* shows reversibility in the presence of crowding agent. However, the forward-scan and reverse-scan of Lyz in Fig. S3d are not perfectly superimposable, indicating that thermal transition for base-denatured Lyz exhibits partial reversibility in presence of crowding agent. On the basis of prior work [94–97], the use of the van't Hoff formalism is valid for the analysis even in cases for where the thermal denaturation of proteins is only partially reversible (*Vide infra*). The thermal transitions of Ferricyt *c* and Lyz are independent on protein concentrations (Fig. S3b,c,e,f).

The thermal denaturation data were analyzed by the Gibbs-Helmholtz Eq. (3) [24]. The $T_m$, $\Delta H_m$ and $\Delta C_p$ values for base-denatured Ferricyt *c* and Lyz obtained in the absence and presence of 300 mg ml$^{-1}$ of dextran 40, dextran 70 and ficoll 70. As concentration of crowding agent is increased from 0.0 to 300 mg ml$^{-1}$, the value of $T_m$ was found to be significantly increased (Table 3). This observation establishes that presence of crowding agent in reaction medium is responsible for increased thermal stability of base-denatured proteins. This is in agreement with previous findings in which crowding agent was found to

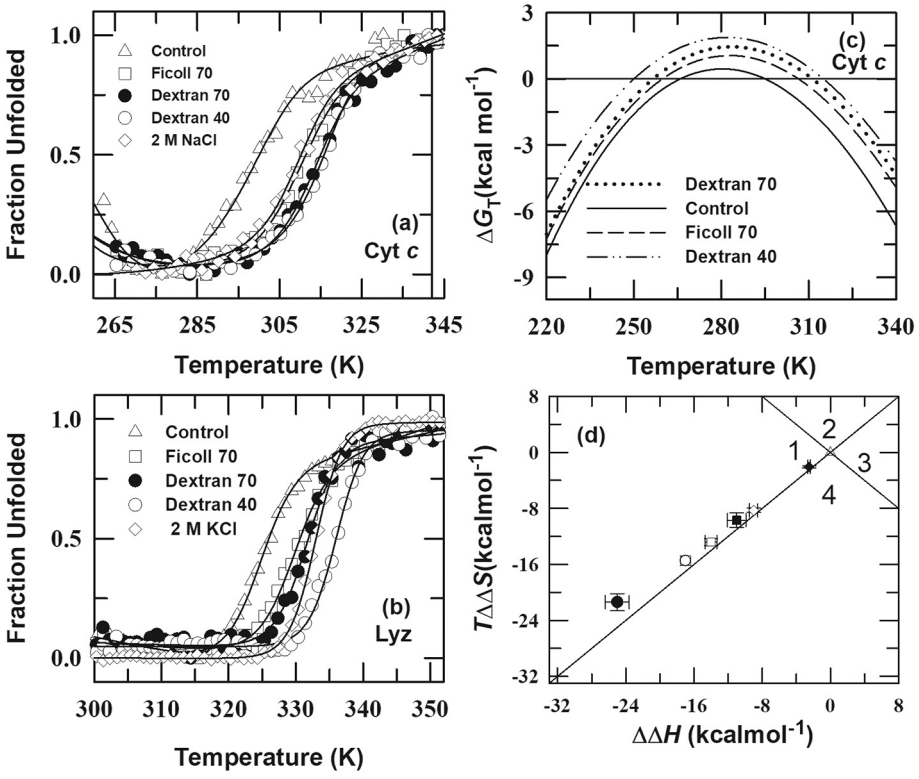


**Fig. 7.** Panels (a) and (b) present the normalized far-UV CD (222 nm) monitored thermal melting curves of alkali-denatured Ferricyt *c* and Lyz at pH 12.9 ( ± 0.1) in the presence of 0.001 M NaCl (Δ), 2.0 M NaCl (for Ferricyt *c*) or 2.0 M KCl (for Lyz) (◊), 300 mg ml$^{-1}$ dextran 40 (o), 300 mg ml$^{-1}$ dextran 70 (●) and 300 mg ml$^{-1}$ ficoll 70 (□), respectively. The continuous lines are fits according to Gibbs-Helmholtz equation (eq. (3)) [24]. Panel (c) presents the temperature dependent stability curves of the base-denatured Ferricyt *c* (pH 12.9 ( ± 0.1)) in the presence of 0.001 M NaCl (solid black line), 300 mg ml$^{-1}$ dextran 40 (long dash line), 300 mg ml$^{-1}$ dextran 70 (dotted line) and 300 mg ml$^{-1}$ ficoll 70 (dash-double dot line), calculated by the use of eq. (7). Panel (d) presents the $T\Delta\Delta S$ *vs* $\Delta\Delta H$ plots for base-denatured proteins at pH 12.9 ( ± 0.1) in the absence (Δ) and presence of ~ 300 mg ml$^{-1}$ of dextran 40 (for Cyt *c* (●), for Lyz (○)), dextran 70 (for Cyt *c* (□), for Lyz (■)) and ficoll 70 (Cyt *c* (◊), for Lyz (♦)).

**Table 3**
Effect of crowding agents on thermodynamic parameters (midpoint temperature ($T_m$), vant Hoff enthalpy ($\Delta H_m$), heat capacity ($\Delta C_p$), free energy of unfolding ($\Delta G_T$), and entropy change (-T$\Delta S_m$) for thermal unfolding (CD 222 nm) of base-denatured Ferricyt *c*, and Lyz at pH 12.9 ( ± 0.1).

| Crowding agents/salt | (crowder) (mg ml$^{-1}$) /Salt (M) | $T_m$ (K) | $\Delta H_m$ (kcal mol$^{-1}$) | $\Delta C_p$ (kcal mol$^{-1}$ K$^{-1}$) | $T_c$ (K) | $\Delta G_T$ (kcal mol$^{-1}$) | $\Delta S_m$ (kcal mol$^{-1}$ K$^{-1}$) | -T$\Delta S_m$ (kcal mol$^{-1}$) |
|---|---|---|---|---|---|---|---|---|
| Ferricyt *c* | | | | | | | | |
| Control | 0.0 | 295.0 | 18.0 | 1.2 | 266 | 0.1 | 0.06 | −17.9 |
| dextran 40 | 300 | 315.0 | 35.0 | 1.0 | 250 | 1.7 | 0.11 | −33.3 |
| dextran 70 | 300 | 311.3 | 32.0 | 1.1 | 256 | 1.3 | 0.11 | −30.7 |
| ficoll 70 | 300 | 306.4 | 27.0 | 1.1 | 260 | 0.9 | 0.09 | −26.2 |
| NaCl | 2.0 | 308.1 | 35.6 | 1.0 | | | | |
| Lyz | | | | | | | | |
| Control | 0.0 | 324.2 | 72.0 | 1.2 | | 5.1 | 0.23 | −66.9 |
| dextran 40 | 300 | 335.9 | 97.0 | 1.3 | | 8.7 | 0.30 | −88.3 |
| dextran 70 | 300 | 331.4 | 83.0 | 1.4 | | 6.4 | 0.26 | −76.6 |
| ficoll 70 | 300 | 329.2 | 74.5 | 1.3 | | 5.5 | 0.24 | −69.0 |
| KCl | 2.0 | 333.9 | 100 | 1.0 | | | | |

*The uncertainty in the values of $T_m$, $\Delta H_m$, $\Delta C_p$, $\Delta G_T$, $\Delta S_m$, and -T$\Delta S_m$ are ± 1.0 K, ± 5.0 kcal mol$^{-1}$, ± 0.3 kcal mol$^{-1}$ K$^{-1}$, ± 3.0 kcal mol$^{-1}$, 0.01 kcal mol$^{-1}$K$^{-1}$and ± 2.0 kcal mol$^{-1}$, respectively.

increase thermal stability of acid-denatured protein [46,98]. The data in Table 3 also reveals that thermal stability of salt (2.0 M NaCl or KCl) and crowding (300 mg ml$^{-1}$) induced MG-states are comparable.

In present study, the crowder-mediated increase in $T_m$ was found to be maximum with Dextran-40 and minimum with Ficoll 70 (dextran 40 > dextran 70 > ficoll 70), suggesting that the nature and shape of crowder or size of crowder of similar shape control the thermal stability of base-denatured proteins. Wittung-Stafshede and co-investigators [79,99,100] demonstrated that for similar shaped crowder, if the protein and crowder are more similar or closer in size then the excluded volume effect will be larger. As compare to cytochrome *c* (12.4 kD) and lysozyme (14.3 kD), dextran 40 is more closer in size than dextran 70 so it exhibits larger excluded volume effect than dextran 70 and therefore dextran 40 produces greater stabilizing effect than dextran 70 on thermal stability of protein. In case of dextran 70 and ficoll 70, dextran 70 has a greater stabilizing effect than ficoll 70 to form MG-states due to the thinner rod shape of dextran 70 compared to ficoll 70 produces larger excluded volume effect.

Previous findings show that the pH-denatured proteins in the presence of low concentrations of salt [24,101,102] and native protein in the presence of denaturant [103] can undergo cold denaturation process. Similarly, the base-denatured Ferricyt *c* exhibits cold denaturation in the presence of 0.01 M NaCl at pH 12.9 ( ± 0.1) (Fig. 7a). However, under the condition employed, the base-denatured Lyz does not exhibit the cold denaturation process (Fig. 7b). Temperature dependent stability curves of base-denatured Ferricyt *c* in the presence of 0.01 M NaCl and with 300 mg ml$^{-1}$ crowding agents (dextran 40, dextran 70, ficoll 70) are shown in Fig. 7c. This observation clearly indicates that with increasing crowding agent concentration, the low temperature unfolding transition of base-denatured Ferricyt *c* becomes less obvious (Fig. 7a and Fig. 7c). The temperature dependent stability curves of different samples were calculated according to

$$\Delta G = \Delta H_m\left(1 - \frac{T}{T_m}\right) + \Delta C_p\left(\left(T\text{-}T_m\right) - T\ln\left(\frac{T}{T_m}\right)\right) \quad (7)$$

The midpoint temperature ($T_m$) for cold denaturation as derived from stability curves of base denatured Ferricyt *c* at different concentration of crowding agents is shown in Table 3. Cold denaturation phenomenon depends upon the thermodynamic principles of protein stability [104,105] and generally arises due to decrease of hydrophobic interactions in proteins at low temperature [106,107]. Interestingly, a few previous reports reveal that not only hydrophobic interaction but also hydrophilic interaction are responsible for cold denaturation [108,109].

According to Daniel Harries formalism, the entropy-enthalpy plots can be used to determine the entropic and enthalpic contributions of crowding agents on stability and folding of proteins [110–112]. In the entropy-enthalpy plots, the diagonal $T\Delta\Delta S = \Delta\Delta H$ represents full compensation between enthalpy and entropy [110]. The area above this diagonal corresponds to cosolute stabilizing effect. In addition, the diagonal $T\Delta\Delta S = -\Delta\Delta H$ further describes the plots into four sectors. Sectors (1 and 2) correspond to stabilizing co-solutes, while other sectors (3 and 4) correspond to destabilizing co-solutes. In addition, sectors (1 and 3) represent the enthalpically dominated effect, while sector (2 and 4) represent entropically dominated effect [111]. The degree of cosolute effect on the free energy is given by the distance from the diagonal, which is the net change in the free energy due to cosolute addition, $\Delta\Delta G = \Delta\Delta H - T\Delta\Delta S$. The current work followed formalism by Daniel Harries and divided the enthalpy-entropy plot into quadrants [110–112]. Fig. 7d describes the $T\Delta\Delta S$ *vs* $\Delta\Delta H$ plots for base-denatured Ferricyt *c* and Lyz at pH 12.9 ( ± 0.1) for three different crowding agents (dextran 40, dextran 70 and ficoll 70). According to pioneer work of Daniel Harries et al., the $T\Delta\Delta S$ *vs* $\Delta\Delta H$ plots in Fig. 7d represent the thermodynamics of folding rather than unfolding [110–112]. The data in Fig. 7d show increase in negative values of both TΔΔS and ΔΔH caused by the crowding agents. These effects almost exactly balance each other in their contributions to $\Delta\Delta G$. The smaller values of $T\Delta S$ (for folding) represent a destabilization (of the molten globule in this case), whereas more negative values of $\Delta H$ represent stabilization. The data points for different crowding agents lie above the upward sloping diagonal in sector 1 (Fig. 7d) suggestive of a predominant enthalpic stabilization. However, most of the sample shows < 0.1 kcal mol$^{-1}$ equivalent of the distances from the diagonal, far less than the reported uncertainties in ΔH (5 kcal mol$^{-1}$, Table 3). Such entropy-entropy compensation is characteristic of processes involving large changes in the interactions between macromolecules and solvent molecules. Overall these results suggest that crowder mediated effect is through changes in water structure or activity and not due to direct interactions with the protein.

Earlier reports documented that the crowder-induced stabilization of proteins by purely steric excluded volume effect is entropic [40,113,114]. However, recent reports concluded that the observed effect of crowding on stability and folding of proteins have a significant enthalpic contributions [115–117]. Furthermore, the enthalpic effect even dominates the entropic one [115–117]. To account for entropic and enthalpic effects of crowders, some recent studies suggested that it is imperative to augment the steric excluded volume effects with other nonspecific interactions [40,115–118]. Therefore, the current study emphasizes that both nonspecific chemical (soft) interactions and hard-core repulsions should be considered to explain the crowder effect on the stability and folding of base-denatured proteins.

### 3.6. Macromolecular crowding constrains the internal dynamics of base-denatured Ferrocyt c-CO

The internal mobility of different states of protein suggests that the MG-state exhibits increased side chains fluctuations compared to native-state [3,5]. However, overall motional freedom of MG-state depends upon the internal dynamic of the denatured state. The previous findings documented that the salt-induced MG-state of base-denatured protein is stiff and dynamically constrained at pH 13 [27,119]. In continuation, the dynamic of MG-state of base-denatured proteins due to crowding agent was examined. The study involved the kinetics of the association of CO with Ferrocyt *c* at pH 12.9 ( ± 0.1) in the absence and presence of different concentrations of crowding agents (dextran 40, dextran 70 and ficoll 70) at 25 °C. The destabilized state of Ferrocyt *c* binds with saturated CO (~1.0 mM) [27,120].

The M80-resident segment of the polypeptide, which is bonded to $Fe^{2+}$ of haem in native/alkaline Ferrocyt *c* [121] but is free in CO bound protein, offer a reacting site for CO association reaction ($Fe^{2+}$–M80 + CO → $Fe^{2+}$–CO + M80). The adjacent residues of M80 have higher thermal factors [122] and the local mobility of the haem ring is suppressed by intrinsic size and rigidity of the ring system [123], so the structural-fluctuation of M80 containing Ω-loop that consists of residues between 70 and 85 is anticipated to be the main factor of CO association to native and alkaline Ferrocyt *c*. An earlier 2D NMR study revealed significantly perturbed residues during CO dissociation spans from residues 80 to 85 [124], which is the main part of Ω-loop [124]. We have previously shown that the decay of peak height for M80 $C_\varepsilon H_3$ resonance (−3.26 ppm) and other side resonance can be used to monitor CO association kinetics of native and alkaline Ferrocyt *c* [71,119]. Thus, the modulation of CO association rate constant of alkaline and native Ferrocyt *c* by crowder reveals the way by which the structural-fluctuation of M80 containing Ω-loop or part of it responds to crowder content in the reaction medium.

The CO association kinetics was monitored (absorbance at 550 nm) with a small volume of CO-saturated aqueous alkaline solution (pH 12.9; ± 0.1) with crowding agent. The α-band (550 nm) of protein Ferrocyt *c* was found to be lost after the formation of Ferrocyt *c* –CO as shown in Fig. 8a [27,71,119]. The kinetics of CO association is well described by a single exponential rate expression with a time constant, $\tau_{ass}$ of ~ 2 min. at pH 12.9 ( ± 0.1), 25 °C. The logarithm of $k_{ass}$ for alkaline Ferrocyt *c* as a function of different concentration of crowding agents at alkaline pH (12.9 ± 0.1) is shown in Fig. 8b and provides an opportunity to analyze the dynamical behavior of the crowding induced MG-state of base-denatured protein. With increased concentration of crowding agent from 0.0 to 300 mg ml$^{-1}$, the log $k_{ass}$ was found to be decreased monoexponentially (Fig. 8b). The crowding-mediated decrease in $k_{ass}$ typically follows the order: dextran 40 > dextran 70 > ficoll 70 (Fig. 8b). This result suggests that nature and shape of crowding agents or size of crowding agent of similar shape control the structural-fluctuation of M80 containing Ω-loop of alkaline Ferrocyt *c*. In addition, the observed kinetic effects could also reflect the overall equilibrium between the denatured state (which would be expected to bind CO very rapidly) and the molten-globule state (which would bind CO much more slowly).

For in-depth analysis of influence of crowding agents on dynamics of alkaline Ferrocyt *c*, the crowding agents dependence of the activation thermodynamic parameters *viz*; activation free energy ($\Delta G^{\ddagger}_{ass}$), activation enthalpy ($\Delta H^{\ddagger}_{ass}$), activation entropy ($\Delta S^{\ddagger}_{ass}$) and entropy change ($-T\Delta S^{\ddagger}_{ass}$) for the CO-association reaction of alkaline Ferrocyt *c* were determined. The Eyring plots were plotted for the CO association reaction of alkaline Ferrocyt *c* in the absence and presence of particular concentration of crowding agent, and CO association to native Ferrocyt *c* in the absence of crowding agents at pH 7.0 (Fig. 8c). These Eyring plots were analyzed by linear least-squares analysis eq. (8) [115] of the temperature dependent $k_{ass}$ using equation given as

$$\ln(k_{ass}h/k_BT) = (\Delta S^{\ddagger}_{ass}/R) - (\Delta H^{\ddagger}_{ass}/RT) \quad (8)$$

The values of $\Delta G^{\ddagger}_{ass}$, $\Delta H^{\ddagger}_{ass}$, $\Delta S^{\ddagger}_{ass}$ and $-T\Delta S^{\ddagger}_{ass}$ for alkaline Ferrocyt *c* in the absence and presence of ~200 mg ml$^{-1}$ of crowding agent are presented in Table 4. If the level of structural fluctuation of Ω-loop is reduced by crowder, the $\Delta H^{\ddagger}_{ass}$ of base-denatured protein with crowder should be relatively higher than without crowder. Interestingly, the value of $\Delta H^{\ddagger}_{ass}$ of base-denatured protein was found to be higher in the presence of crowding agent than denatured protein without crowding agent

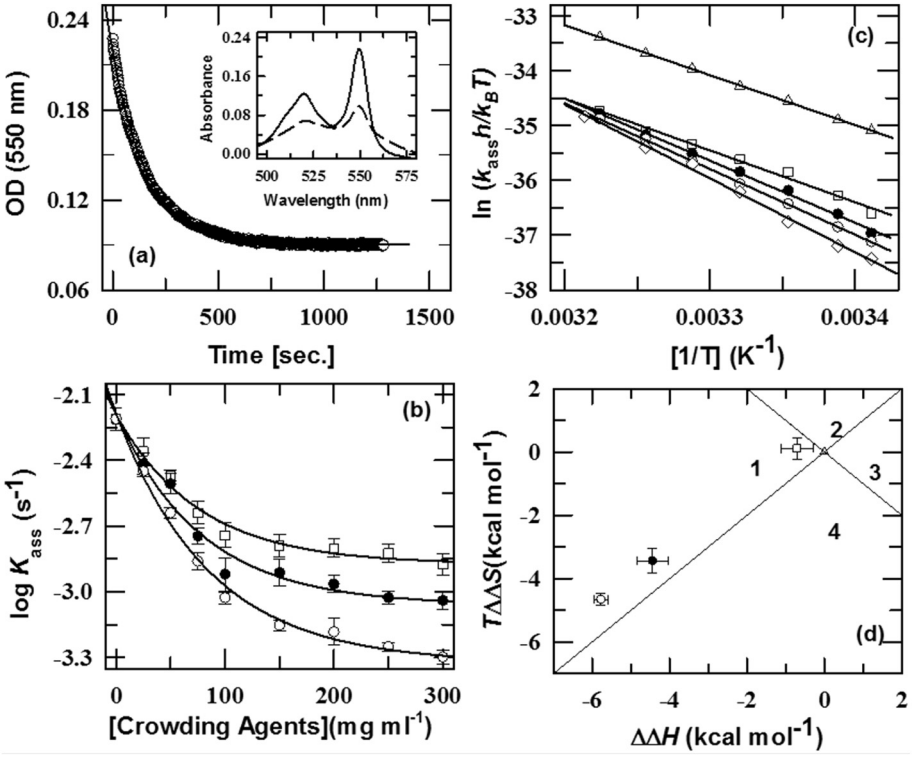


**Fig. 8.** Panel (a) presents the representative slow single-phase CO-association kinetic trace of alkaline Ferrocyt *c* (τ = 2.0 min in the absence of crowding agent at pH 12.9 ( ± 0.1), 25 °C). Inset of panel (a) presents the steady-state visible absorption spectra of Ferrocyt *c* (solid line) and Ferrocyt *c*-CO (dash line) at 25 °C, pH 12.9 ( ± 0.1) in 2 mM CAPS-buffer. Panel (b) shows dependence of the rate of CO association of alkaline Ferrocyt *c* (pH 12.9) with dextran 40 (o), dextran 70 (●), ficoll 70 (□) at 25 °C. The lines through the data have been drawn by inspection only. (c) Eyring plot for the CO association reaction of alkaline Ferrocyt *c* at pH 12.9 ( ± 0.1); in the absence of crowding agents (Δ); in the presence of 200 mg ml$^{-1}$ dextran 40 (o); 200 mg ml$^{-1}$ dextran 70 (●); 200 mg ml$^{-1}$ ficoll 70 (□) and at pH 7 in the absence of crowding agents (◊). Eyring plots were analyzed by linear least-squares analysis (eq. (8)) [98,100]. The $T\Delta\Delta S$ and $\Delta\Delta H$ plot for different crowders. Data points correspond to in the absence (Δ) and presence of 200 mg ml$^{-1}$ of dextran 40 (o), dextran 70 (●) and ficoll 70 (□) for Ferrocyt *c* at pH 12.9 ( ± 0.1).

**Table 4**
The effect of crowding agents on activation thermodynamic parameters for CO-association reaction of Ferrocyt *c* at pH 12.9 ( ± 0.1)*.

| Additives | Conc. (mg ml$^{-1}$) | $\Delta G_{ass}^{\ddagger}$ (kcal mol$^{-1}$) | $\Delta H_{ass}^{\ddagger}$ (kcal mol$^{-1}$) | $\Delta S_{ass}^{\ddagger}$ (cal mol$^{-1}$ K$^{-1}$) | $-T\Delta S_{ass}^{\ddagger}$ (kcal mol$^{-1}$ K$^{-1}$) |
|---|---|---|---|---|---|
| Control | 0.0 | 20.6 (0.05) | 18.2 (0.2) | −8.1 (0.6) | 2.4 (0.2) |
| dextran 40 | 200 | 21.7 (0.06) | 24.0 (0.2) | 7.5 (0.6) | −2.2 (0.2) |
| dextran 70 | 200 | 21.6 (0.05) | 22.6 (0.6) | 3.4 (1.8) | −1.0 (0.5) |
| ficoll 70 | 200 | 21.4 (0.08) | 18.9 (0.9) | −8.5 (3.0) | 2.5 (0.9) |
| Control (pH 7) | 0.0 | 22.0 (0.1) | 26.0 (0.1) | 12.4 (0.8) | −3.7 (0.2) |

Activation free energy ($\Delta G_{ass}^{\ddagger}$) and entropy changes ($-T\Delta S_{ass}^{\ddagger}$) are given at 25 °C.
* The uncertainties (standard error) in $\Delta G_{ass}^{\ddagger}$, $\Delta H_{ass}^{\ddagger}$, $-T\Delta S_{ass}^{\ddagger}$ and $\Delta S_{ass}^{\ddagger}$ are indicated in parenthesis.

(Table 4). In contrast, the value of $\Delta H_{ass}^{\ddagger}$ of base-denatured protein in the presence of crowding agents was found to be lower than the native protein at pH 7.0 (Table 4). These results clearly indicate that the level of structural fluctuation of Ω-loop of base-denatured protein in the presence of crowding agent is more reduced relative to that in the absence of crowding agents but found to be increased than the native state (Table 4). A recent report by Krishnamoorthy et al. showed that the macromolecular crowding restricts the internal dynamics of barstar [125].

The increase of $\Delta H_{ass}^{\ddagger}$ due to crowding agents (dextran 40, dextran 70 and ficoll 70) was found to be accompanied by a decrease in the entropy change– $T\Delta S_{ass}^{\ddagger}$as represented in Table 4. The $T\Delta\Delta S$ *vs* $\Delta\Delta H$ plots for alkaline Ferrocyt *c* in absence and presence of dextran 40, dextran 70 and ficoll 70 at pH 12.9 ( ± 0.1) are shown in Fig. 8d. The data points for crowders lie in sector 1 (Fig. 8d), consistent with the models describes enthalpically dominated stabilization [110–112].

## 4. Conclusion

The high concentrations of crowding agents transform the base-denatured Ferricyt *c* and Lyz to MG-states at alkaline pH (12.9; ± 0.1). The crowding-mediated stabilization and refolding of base-denatured Ferricyt *c* and Lyz to MG-states were found to be dependent on the nature and shape of crowding agents or on size of crowding agents of similar shape. The crowder-induced MG-states of base-denatured Ferricyt *c* and Lyz resemble the generic properties of MG-states. ANS binding experiments also provided the evidence that the crowder environment transforms the base-denatured Ferricyt *c* and Lyz into MG-states. Data analysis of the thermal denaturation curves of base-denatured Ferricyt *c* and Lyz under different concentration of dextran 40, dextran 70 and ficoll 70 revealed that (i) the base-denatured Ferricyt *c* exhibits cold denaturation, (ii) crowder environment increases the thermal stability of base-denatured proteins, and (iii) nature and shape of crowding agents or size of crowding agents of similar shape modulate the crowding-mediated increase in thermal stability of base-denatured proteins, and (iv) crowding-mediated increase in thermal stability of base-denatured proteins resulted from enthalpy-entropy compensation. Analysis of kinetic and thermodynamic parameters measured for CO association reaction of alkaline Ferrocyt *c* at pH 12.9 ( ± 0.1) under different concentrations of dextran 70, dextran 40 and ficoll 70 revealed that (i) crowder environment reduces the level of structural fluctuation of M80 containing Ω-loop of base-denatured Ferrocyt *c*-CO, (ii) nature and shape of crowding agents or size of crowding agents of similar shape modulate the crowding-mediated decreases in the level of structural fluctuation of M80 containing Ω-loop of base-denatured Ferrocyt *c*-CO, and (iii) crowding-mediated decreases in the level of structural fluctuation of M80 containing Ω-loop of base-denatured Ferrocyt *c*-CO is enthalpically dominated than the entropically.

## Acknowledgements

This work was supported by DBT grant (BT/PR11684/BRB/10/1300/2014), DST-SERB grant (EMR/2014/000242) and ICMR grant (F.No. 52/6/2013-BMS), Government of India.

## Author contributions

R.K*. conceived the ideas. R.K., D.S., and R.K*. designed the research. R.K. M.K. performed the research. R.K*., M.K. D.S., M.G., V.K. and R.K analyzed the data. R.K., M.G., D.S., V.K., and R.K.* wrote the paper.

## Appendix A. Supplementary data

Supplementary data to this article can be found online at https://doi.org/10.1016/j.bbapap.2018.08.012.

## References

[1] P.G. Wolynes, J.N. Onuchic, D. Thirumalai, Navigating the folding routes, Science 267 (1995) 1619–1620.
[2] O.B. Ptitsyn, How the molten globule became, Trends Biochem. Sci. 20 (1995) 376–379.
[3] D. Dolgikh, R. Gilmanshin, E. Brazhnikov, V. Bychkova, G. Semisotnov, S.Y. Venyaminov, O. Ptitsyn, α-Lactalbumin: compact state with fluctuating tertiary structure? FEBS Lett. 136 (1981) 311–315.
[4] M. Ohgushi, A. Wada, 'Molten-globule state': a compact form of globular proteins with mobile side-chains, FEBS Lett. 164 (1983) 21–24.
[5] D. Dolgikh, L. Abaturov, I. Bolotina, E. Brazhnikov, V. Bychkova, R. Gilmanshin, Y.O. Lebedev, G. Semisotnov, E. Tiktopulo, O. Ptitsyn, Compact state of a protein molecule with pronounced small-scale mobility: bovine α-lactalbumin, Eur. Biophys. J. 13 (1985) 109–121.
[6] K. Kamagata, M. Arai, K. Kuwajima, Unification of the folding mechanisms of non-two-state and two-state proteins, J. Mol. Biol. 339 (2004) 951–965.
[7] M. Arai, and K. Kuwajima, Role of the molten globule state in protein folding, Adv. Protein Chem. 53 (2000) 209–282.
[8] O.B. Ptitsyn, Protein folding: hypotheses and experiments, J. Protein Chem. 6 (1987) 273–293.
[9] Y.V. Griko, P.L. Privalov, Thermodynamic puzzle of apomyoglobin unfolding, J. Mol. Biol. 235 (1994) 1318–1325.
[10] K. Shirahama, K. Tsujii, T. Takagi, Free-boundary electrophoresis of sodium dodecyl sulfate-protein polypeptide complexes with special reference to SDS-polyacrylamide gel electrophoresis, J. Biochem. 75 (1974) 309–319.
[11] N.C. Robinson, C. Tanford, The binding of deoxycholate, Triton X-100, sodium dodecyl sulfate, and phosphatidylcholine vesicles to cytochrome b5, Biochemistry 14 (1975) 369–378.
[12] V.E. Bychkova, R.H. Pain, O.B. Ptitsyn, The 'molten globule'state is involved in the translocation of proteins across membranes? FEBS Lett. 238 (1988) 231–234.
[13] F.G. van der Goot, J.H. Lakey, F. Pattus, The molten globule intermediate for protein insertion or translocation through membranes, Trends Cell Biol. 2 (1992) 343–348.
[14] S. Banuelos, A. Muga, Binding of molten globule-like conformations to lipid bilayers structure of native and partially folded α-lactalbumin bound to model membranes, J. Biol. Chem. 270 (1995) 29910–29915.
[15] E.A. Bryson, S.E. Rankin, M. Carey, A. Watts, T.J. Pinheiro, Folding of apocytochrome c in lipid micelles: Formation of α-helix precedes membrane insertion, J. Biol. Inorg. Chem. 38 (1999) 9758–9767.
[16] K.-I. Nakayama, S. Hatakeyama, K. Nakayama, Regulation of the cell cycle at the G1–S transition by proteolysis of cyclin E and p27Kip1, Biochem. Biophys. Res. Commun. 282 (2001) 853–860.
[17] A.K. Dunker, M.S. Cortese, P. Romero, L.M. Iakoucheva, V.N. Uversky, Flexible nets. The roles of intrinsic disorder in protein interaction networks, FEBS J. 272 (2005) 5129–5148.
[18] E. Kókai, Á. Tantos, E. Vissi, B. Szöőr, P. Tompa, J. Gausz, L. Alphey, P. Friedrich, V. Dombrádi, CG15031/PPYR1 is an intrinsically unstructured protein that interacts with protein phosphatase Y, Arch. Biochem. Biophys. 451 (2006) 59–67.
[19] P. Radivojac, S. Vucetic, T. R. O'Connor, V. N. Uversky, Z. Obradovic, and A. K. Dunker, Calmodulin signaling: Analysis and prediction of a disorder-dependent molecular recognition, Proteins 63 (2006) 398–410.
[20] P. Tompa, P. Bánki, M. Bokor, P. Kamasa, D. Kovács, G. Lasanda, K. Tompa,

Protein-water and protein-buffer interactions in the aqueous solution of an intrinsically unstructured plant dehydrin: NMR intensity and DSC aspects, Biophys. J. 91 (2006) 2243–2249.
[21] B.Y. Baker, D.C. Yaworsky, W.L. Miller, A pH-dependent molten globule transition is required for activity of the steroidogenic acute regulatory protein, StAR, J. Biol. Chem. 280 (2005) 41753–41760.
[22] L. Chen, V. Balabanidou, D.P. Remeta, C.A. Minetti, A.G. Portaliou, A. Economou, C.G. Kalodimos, Structural instability tuning as a regulatory mechanism in protein-protein interactions, Mol. Cell 44 (2011) 734–744.
[23] M. Kjaergaard, K. Teilum, F.M. Poulsen, Conformational selection in the molten globule state of the nuclear coactivator binding domain of CBP, Proc. Natl. Acad. Sci. U. S. A. 107 (2010) 12535–12540.
[24] R. Kumar, N.P. Prabhu, D.K. Rao, A.K. Bhuyan, The alkali molten globule state of horse ferricytochrome c: observation of cold denaturation, J. Mol. Biol. 364 (2006) 483–495.
[25] S. Nakamura, T. Baba, S. Kidokoro, A molten globule-like intermediate state detected in the thermal transition of cytochrome c under low salt concentration, Biophys. Chem. 127 (2007) 103–112.
[26] S. Nakamura, S. Kidokoro, Direct observation of the enthalpy change accompanying the native to molten-globule transition of cytochrome c by using isothermal acid-titration calorimetry, Biophys. Chem. 113 (2005) 161–168.
[27] D.K. Rao, R. Kumar, M. Yadaiah, A.K. Bhuyan, The alkali molten globule state of ferrocytochrome c: extraordinary stability, persistent structure, and constrained overall dynamics, Biochemistry 45 (2006) 3412–3420.
[28] B.R. Rami, G. Krishnamoorthy, J.B. Udgaonkar, Dynamics of the core tryptophan during the formation of a productive molten globule intermediate of barstar, Biochemistry 42 (2003) 7986–8000.
[29] B.R. Rami, J.B. Udgaonkar, Mechanism of formation of a productive moltenglobule form of barstar, Biochemistry 41 (2002) 1710–1716.
[30] P.R. Davis-Searles, A.S. Morar, A.J. Saunders, D.A. Erie, G.J. Pielak, Sugar-induced molten-globule model, Biochemistry 37 (1998) 17048–17053.
[31] A.J. Saunders, P.R. Davis-Searles, D.L. Allen, G.J. Pielak, D.A. Erie, Osmolyte-induced changes in protein conformational equilibria, Biopolymers 53 (2000) 293–307.
[32] T. Kamiyama, Y. Sadahide, Y. Nogusa, K. Gekko, Polyol-induced molten globule of cytochrome c: an evidence for stabilization by hydrophobic interaction, Biochim. Biophys. Acta 1434 (1999) 44–57.
[33] S. Nakamura, Y. Seki, E. Katoh, S. Kidokoro, Thermodynamic and structural properties of the acid molten globule state of horse cytochrome c, Biochemistry 50 (2011) 3116–3126.
[34] L.F.S. Mendes, A.F. Garcia1, P.S. Kumagai, F.R. de Morais, F.A. Melo, L. Kmetzsch, M.H. Vainstein, M.L. Rodrigues, A.J. Costa-Filho, New structural insights into Golgi Reassembly, Stacking Protein, (GRASP) in solution, Sci, Report 6 (2016) 29976.
[35] K. Nasreen, S. Ahamad, F. Ahmad, I. Hassan, A. Islam, Macromolecular crowding induces molten globule state in the native myoglobin at physiological pH, Int. J. Biol. Macromol. 106 (2018) 130–139.
[36] Z.A. Parray, S. Shahid, F. Ahmad, M.I. Hassan, A. Islam, Characterization of intermediate state of myoglobin in the presence of PEG 10 under physiological conditions, Int. J. Biol. Macromol. 99 (2017) 241–248.
[37] M.A. Dar, M.A. Wahiduzzaman, D. Haque, M.I. Idrees, A. Hassan, F. Islam, Ahmad, Characterization of folding intermediates during urea-induced denaturation of human carbonic anhydrase II, Int. J. Biol. Macromol. 95 (2017) 881–887.
[38] L. Stagg, S.Q. Zhang, M.S. Cheung, P. Wittung-Stafshede, Molecular crowding enhances native structure and stability of α/β protein flavodoxin, Proc. Natl. Acad. Sci. U. S. A. 104 (2007) 18976–18981.
[39] M.S. Cheung, D. Klimov, D. Thirumalai, Molecular crowding enhances native state stability and refolding rates of globular proteins, Proc. Natl. Acad. Sci. U. S. A. 102 (2005) 4753–4758.
[40] Y. Wang, M. Sarkar, A.E. Smith, A.S. Krois, G.J. Pielak, Macromolecular crowding and protein stability, J. Am. Chem. Soc. 134 (2012) 16614–16618.
[41] M. Erlkamp, S. Grobelny, R. Winter, Crowding effects on the temperature and pressure dependent structure, stability and folding kinetics of Staphylococcal Nuclease, Phys. Chem. Chem. Phys. 16 (2014) 5965–5976.
[42] M.S. Cheung, D. Thirumalai, Effects of crowding and confinement on the structures of the transition state ensemble in proteins, J. Phys. Chem. B 111 (2007) 8250–8257.
[43] Y. Zhai, R. Winter, Effect of Molecular Crowding on the Temperature–pressure Stability Diagram of Ribonuclease a, ChemPhysChem 14 (2013) 386–393.
[44] A. Christiansen, P. Wittung-Stafshede, Synthetic crowding agent dextran causes excluded volume interactions exclusively to tracer protein apoazurin, FEBS Lett. 588 (2014) 811–814.
[45] D.L. Pincus, C. Hyeon, D. Thirumalai, Effects of trimethylamine N-oxide (TMAO) and crowding agents on the stability of RNA hairpins, J. Am. Chem. Soc. 130 (2008) 7364–7372.
[46] K. Sasahara, P. McPhie, A.P. Minton, Effect of dextran on protein stability and conformation attributed to macromolecular crowding, J. Mol. Biol. 326 (2003) 1227–1237.
[47] D.M. Hatters, A.P. Minton, G.J. Howlett, Macromolecular crowding accelerates amyloid formation by human apolipoprotein C-II, J. Biol. Chem. 277 (2002) 7824–7830.
[48] E.E. Wanker, Protein aggregation in Huntington's and Parkinson's disease: implications for therapy, Mol. Med. Today 6 (2000) 387–391.
[49] L. Breydo, K.D. Reddy, A. Piai, I.C. Felli, R. Pierattelli, V.N. Uversky, The crowd you're in with: effects of different types of crowding agents on protein aggregation, Biochim. Biophys. Acta 1844 (2014) 346–357.
[50] S. Mittal, L.R. Singh, Macromolecular crowding decelerates aggregation of a β-rich protein, bovine carbonic anhydrase: a case study, J. Biochem. 156 (2014) 273–282.
[51] R.J. Ellis, A.P. Minton, Protein aggregation in crowded environments, Biol. Chem. 387 (2006) 485–497.
[52] B. van den Berg, R.J. Ellis, C.M. Dobson, Effects of macromolecular crowding on protein folding and aggregation, EMBO J. 18 (1999) 6927–6933.
[53] R. Engel, A.H. Westphal, D.H. Huberts, S.M. Nabuurs, S. Lindhoud, A.J. Visser, C.P. van Mierlo, Macromolecular crowding compacts unfolded apoflavodoxin and causes severe aggregation of the off-pathway intermediate during apoflavodoxin folding, J. Biol. Chem. 283 (2008) 27383–27394.
[54] J. Li, S. Zhang, C. Wang, Effects of macromolecular crowding on the refolding of glucose-6-phosphate dehydrogenase and protein disulfide isomerase, J. Biol. Chem. 276 (2001) 34396–34401.
[55] S.L. Flaugh, K.J. Lumb, Effects of macromolecular crowding on the intrinsically disordered proteins c-Fos and p27Kip1, Biomacromolecules 2 (2001) 538–540.
[56] M.M. Dedmon, C.N. Patel, G.B. Young, G.J. Pielak, FlgM gains structure in living cells, Proc. Natl. Acad. Sci. U. S. A. 99 (2002) 12681–12684.
[57] A. Minton, J. Wilf, Effect of macromolecular crowding upon the structure and function of an enzyme: glyceraldehyde-3-phosphate dehydrogenase, Biochemistry 20 (1981) 4821–4826.
[58] A.P. Minton, The effect of volume occupancy upon the thermodynamic activity of proteins: some biochemical consequences, Mol. Cell. Biochem. 55 (1983) 119–140.
[59] G. Ralston, Effects of crowding in protein solutions, J. Chem. Educ. 67 (1990) 857.
[60] S.B. Zimmerman, A.P. Minton, Macromolecular crowding: biochemical, biophysical, and physiological consequences, Annu. Rev. Biophys. Biomol. Struct. 22 (1993) 27–65.
[61] A.P. Minton, Molecular crowding: analysis of effects of high concentrations of inert cosolutes on biochemical equilibria and rates in terms of volume exclusion, Methods Enzymol. 295 (1998) 127–149.
[62] A.P. Minton, Effect of a concentrated “inert” macromolecular cosolute on the stability of a globular protein with respect to denaturation by heat and by chaotropes: a statistical-thermodynamic model, Biophys. J. 78 (2000) 101–109.
[63] A.P. Minton, The influence of macromolecular crowding and macromolecular confinement on biochemical reactions in physiological media, J. Biol. Chem. 276 (2001) 10577–10580.
[64] H. Theorell, Å. Åkesson, Studies on cytochrome c. II. The optical properties of pure cytochrome c and some of its derivatives, J. Am. Chem. Soc. 63 (1941) 1812–1818.
[65] L. Bancil, L. Bertini, K. Bren, H.B. Gray, P. Turano, pH-dependent equilibria of yeast Met80Ala-iso-1-cytochrome *c* probed by NMR spectroscopy: a comparison with the wild-type protein, Chem. Biol. 2 (1995) 377–383.
[66] S. Dopner, J. Hudecek, B. Ludwig, H. Witt, P. Hildebrandt, Structural changes in cytochrome cytochrome c oxidase induced by cytochrome c binding. A resonance Raman study, Biochim. Biophys. Acta 1480 (2000) 57–64.
[67] K.E. Falk, J. Angstrom, $^{1}$H NMR longitudinal relaxation study of the interaction between cytochrome c and cytochrome c oxidase, Biochim. Biophys. Acta 722 (1983) 291–296.
[68] S. Soussi, A.C. Bylund-Fellenius, T. Schersten, J. Angstrom, $^{1}$H NMR evaluation of the ferricytochrome c-cardiolipin interaction. Effect of superoxide radicals, Biochem. J. 265 (1990) 227–232.
[69] P. Hildebrandt, F. Vanhecke, G. Buse, T. Soulimane, A.G. Mauk, Resonance Raman study of the interactions between cytochrome c variants and cytochrome c oxidase, Biochemistry 32 (1993) 10912–10922.
[70] P. Hildebrandt, T. Heimburg, T., D. Marsh, Quantitative conformational analysis of cytochrome c bound to phospholipid vesicles studied by resonance Raman spectroscopy. Eur. J. Biophys. 18 (1990)193–201.
[71] R. Kumar, N.P. Prabhu, M. Yadaiah, A.K. Bhuyan, Protein stiffening and entropic stabilization in the subdenaturing limit of guanidine hydrochloride, Biophys. J. 87 (2004) 2656–2662.
[72] R. Kumar, Analysis of the pH-dependent thermodynamic stability, local motions, and microsecond folding kinetics of carbonmonoxycytochrome c, Arch. Biochem. Biophys. 606 (2016) 16–25.
[73] R. Kumar, N.P. Prabhu, A.K. Bhuyan, Ultrafast events in the folding of ferrocytochrome c, Biochemistry 44 (2005) 9359–9367.
[74] A.K. Bhuyan, The off-pathway status of the alkali molten globule is unrelated to heme misligation and trans-pH effects: experiments with ferrocytochrome c, Biochemistry 49 (2010) 7774–7782.
[75] J.M. Vanderkooi, M. Erecinska, Cytochrome c interaction with membranes, Eur. J. Biochem. 60 (1975) 199–207.
[76] T.Y. Tsong, The Trp-59 fluorescence of ferricytochrome c as a sensitive measure of the over-all protein conformation, J. Biol. Chem. 249 (1974) 1988–1990.
[77] S. Lehrer, G.D. Fasman, Fluorescence of lysozyme and lysozyme substrate complexes separation of tryptophan contributions by fluorescence difference methods, J. Biol. Chem. 242 (1967) 4644–4651.
[78] M. Ansari, S. Zubair, S. Atif, M. Kashif, N. Khan, M. Rehan, T. Anwar, A. Iqbal, M. Owais, Identification and characterization of molten globule-like state of hen egg-white lysozyme in presence of salts under alkaline conditions, Protein Pept. Lett. 17 (2010) 11–17.
[79] A. Christiansen, Q. Wang, A. Samiotakis, M.S. Cheung, P. Wittung-Stafshede, Factors defining effects of macromolecular crowding on protein stability: an in vitro/in silico case study using cytochrome c, Biochemistry 49 (2010) 6519–6530.
[80] O. Ptitsyn, Molten globule and protein folding, Adv. Protein Chem. 47 (1995) 83–229.
[81] O.K. Gasymov, B.J. Glasgow, ANS fluorescence: potential to augment the

identification of the external binding sites of proteins, Biochim. Biophys. Acta 1774 (2007) 403–411.
[82] M. Engelhard, P.A. Evans, Kinetics of interaction of partially folded proteins with a hydrophobic dye: evidence that molten globule character is maximal in early folding intermediates, Protein Sci. 4 (1995) 1553–1562.
[83] V.N. Uversky, S. Winter, G. Löber, Use of fluorescence decay times of 8-ANS-protein complexes to study the conformational transitions in proteins which unfold through the molten globule state, Biophys. Chem. 60 (1996) 79–88.
[84] E. Schönbrunn, S. Eschenburg, K. Luger, W. Kabsch, N. Amrhein, Structural basis for the interaction of the fluorescence probe 8-anilino-1-naphthalene sulfonate (ANS) with the antibiotic target MurA, Proc. Natl. Acad. Sci. U. S. A. 97 (2000) 6345–6349.
[85] G. Semisotnov, N. Rodionova, O. Razgulyaev, V. Uversky, A. Gripas, R. Gilmanshin, Study of the "molten globule" intermediate state in protein folding by a hydrophobic fluorescent probe, Biopolymers 31 (1991) 119–128.
[86] K. Kuwajima, E.P. Garvey, B.E. Finn, C.R. Matthews, S. Sugai, Transient intermediates in the folding of dihydrofolate reductase as detected by far-ultraviolet circular dichroism spectroscopy, Biochemistry 30 (1991) 7693–7703.
[87] A. Arroyo-Reyna, A. Hernandez-Arana, R. Arreguin-Espinosa, Circular dichroism of stem bromelain: a third spectral class within the family of cysteine proteinases, Biochemistry 300 (1994) 107–110.
[88] Y. Goto, L.J. Calciano, A.L. Fink, Acid-induced folding of proteins, Proc. Natl. Acad. Sci. U. S. A. 87 (1990) 573–577.
[89] S.Y. Venyaminov, J.T. Yang, Determination of protein secondary structure, Circular Dichroism and the Conformational Analysis of Biomolecules, Springer, 1996, pp. 69–107.
[90] A. Naiyer, M.I. Hassan, A. Islam, M. Sundd, F. Ahmad, Structural characterization of MG and pre-MG states of proteins by MD simulations, NMR, and other techniques, J. Biomol. Struct. Dyn. 33 (2015) (2015) 2267–2284.
[91] M. Kataoka, Y. Hagihara, K. Mihara, Y. Goto, Molten globule of cytochrome c studied by small angle X-ray scattering, J. Mol. Biol. 229 (1993) 591–596.
[92] Y. Goto, Y. Hagihara, D. Hamada, M. Hoshino, I. Nishii, Acid-induced unfolding and refolding transitions of cytochrome c: a three-state mechanism in water and deuterium oxide, Biochemistry 32 (1993) 11878–11885.
[93] C. Pace, J. Hermans, The stability of globular protein, Crit. Rev. Biochem. 3 (1975) 1–43.
[94] M.T. Fisher, Differences in thermal stability between reduced and oxidized cytochrome b-562 from Escherichia coli, Biochemistry 30 (1991) 10012–10018.
[95] S.P. Manly, K.S. Matthews, J.M. Sturtevant, Thermal denaturation of the core protein of lac repressor, Biochemistry 24 (1985) 3842–3846.
[96] V. Edge, N.M. Allewell, J.M. Sturtevant, High-resolution differential scanning calorimetric analysis of the subunits of Escherichia coli aspartate transcarbamoylase, Biochemistry 24 (1985) 5899–5906.
[97] C.Q. Hu, J.M. Sturtevant, Thermodynamic study of yeast phosphoglycerate kinase, Biochemistry 26 (1987) 178–182.
[98] P. McPhie, Y.-s. Ni, A.P. Minton, Macromolecular crowding stabilizes the molten globule form of apomyoglobin with respect to both cold and heat unfolding, J. Mol. Biol. 361 (2006) 7–10.
[99] T. Mikaelsson, J. Adén, L.B. Johansson, P. Wittung-Stafshede, Direct observation of protein unfolded state compaction in the presence of macromolecular crowding, Biophys. J. 104 (2013) 694–704.
[100] A. Christiansen, P. Wittung-Stafshede, Quantification of excluded volume effects on the folding landscape of *Pseudomonas aeruginosa* apoazurin in vitro, Biophys. J. 105 (2013) 1689–1699.
[101] P.L. Privalov, Cold denaturation of protein, Crit. Rev. Biochem. Mol. Biol. 25 (1990) 281–306.
[102] I. Nishii, M. Kataoka, F. Tokunaga, Y. Goto, Cold denaturation of the molten globule states of apomyoglobin and a profile for protein folding, Biochemistry 33 (1994) 4903–4909.
[103] V.R. Agashe, J.B. Udgaonkar, Thermodynamics of denaturation of barstar: evidence for cold denaturation and evaluation of the interaction with guanidine hydrochloride, Biochemistry 34 (1995) 3286–3299.
[104] P.L. Privalov, Stability of proteins small globular proteins, Adv. Protein Chem. 33 (1979) 167–241.
[105] W.J. Becktel, J.A. Schellman, Protein stability curves, Biopolymers 26 (1987) 1859–1877.
[106] K.P. Murphy, E. Freire, Thermodynamics of structural stability and cooperative folding behavior in proteins, Adv. Protein Chem. 43 (1992) 313–361.
[107] G.I. Makhatadze, P.L. Privalov, Energetics of protein structure, Adv. Protein Chem. 47 (1995) 307–425.
[108] R.S. Spolar, J.R. Livingstone, M.T. Record Jr., Use of liquid hydrocarbon and amide transfer data to estimate contributions to thermodynamic functions of protein folding from the removal of nonpolar and polar surface from water, Biochemistry 31 (1992) 3947–3955.
[109] R.S. Spolar, M.T. Record Jr., Coupling of Local Folding to Site—specific Binding of proteins to DNA, Science 263 (1994) 777–784.
[110] S. Sukenik, L. Sapir, D. Harries, Balance of enthalpy and entropy in depletion forces, Curr. Opin. Colloid Interface Sci. 18 (2013) 495–501.
[111] L. Sapir, D. Harries, Is the depletion force entropic? Molecular crowding beyond steric interactions, Curr. Opin. Colloid Interface Sci. 20 (2015) 3–10.
[112] L. Sapir, D. Harries, Origin of enthalpic depletion forces, J. Phys. Chem. Lett. 5 (2014) 1061–1065.
[113] A.P. Minton, Quantitative assessment of the relative contributions of steric repulsion and chemical interactions to macromolecular crowding, Biopolymers 99 (2013) 239–244.
[114] H.-X. Zhou, Polymer crowders and protein crowders act similarly on protein folding stability, FEBS Lett. 587 (2013) 394–397.
[115] R. Kumar, D. Sharma, R. Jain, S. Kumar, Role of macromolecular crowding and salt ions on the structural-fluctuation of a highly compact configuration of carbonmonoxycytochrome c, Biophys. Chem. 207 (2015) 61–73.
[116] M. Senske, L. Törk, B. Born, M. Havenith, C. Herrmann, S. Ebbinghaus, Protein stabilization by macromolecular crowding through enthalpy rather than entropy, Acc. Chem. Res. 136 (2014) 9036–9041.
[117] L.A. Benton, A.E. Smith, G.B. Young, G.J. Pielak, Unexpected effects of macromolecular crowding on protein stability, Biochemistry 51 (2012) 9773–9775.
[118] A.P. Minton, Explicit Incorporation of Hard and Soft Protein-Protein Interactions into Models for Crowding Effects in Protein Mixtures. II. Effects of varying Hard and Soft Interactions upon Prototypical Chemical Equilibria, J. Phys. Chem. B 121 (2017) 5515–5522.
[119] R. Jain, S. Kaur, R. Kumar, Guanidine hydrochloride-induced alkali molten globule model of horse ferrocytochrome c, J. Biochem. 153 (2013) 161–177.
[120] A.K. Bhuyan, R. Kumar, Kinetic barriers to the folding of horse cytochrome c in the reduced state, Biochemistry 41 (2002) 12821–12834.
[121] J.F. Leszczynski, G.D. Rose, Loops in globular proteins: a novel category of secondary structure, Science 234 (1986) 849–855.
[122] A.M. Berghuis, G.D. Brayer, Oxidation state-dependent conformational changes in cytochrome c, J. Mol. Biol. 223 (1992) 959–976.
[123] J.D. Morgan, J. Andrew McCammon, S.H. Northrup, Molecular dynamics of ferrocytochrome c: time dependence of the atomic displacements, Biopolymers 22 (1983) 1579–1593.
[124] R.F. Latypov, K. Maki, H. Cheng, S.D. Luck, H. Roder, Folding mechanism of reduced cytochrome c: equilibrium and kinetic properties in the presence of carbon monoxide, J. Mol. Biol. 383 (2008) 437–453.
[125] S. Mondal, M.V. Kallianpur, J.B. Udgaonkar, G. Krishnamoorthy, Molecular crowding causes narrowing of population heterogeneity and restricts internal dynamics in a protein, Methods Appl Fluoresc 4 (2015) 014003.